Dirac electrons in graphene-based quantum wires and quantum dots

2009 J. Phys.: Condens. Matter 21 344202

(http://iopscience.iop.org/0953-8984/21/34/344202)

J. Phys.: Condens. Matter **21** (2009) 344202 (18pp) doi:10.1088/0953-8984/21/34/344202

Dirac electrons in graphene-based quantum wires and quantum dots

N M R Peres[1], J N B Rodrigues[2], T Stauber[1] and J M B Lopes dos Santos[2]

[1] Centro de Física e Departamento de Física, Universidade do Minho, P-4710-057, Braga, Portugal
[2] CFP and Departamento de Física, Faculdade de Ciências Universidade do Porto, P-4169-007, Porto, Portugal

Received 2 October 2008, in final form 5 December 2008
Published 27 July 2009
Online at stacks.iop.org/JPhysCM/21/344202

Abstract

In this paper we analyse the electronic properties of Dirac electrons in finite-size ribbons and in circular and hexagonal quantum dots. We show that due to the formation of sub-bands in the ribbons it is possible to spatially localize some of the electronic modes using a p–n–p junction. We also show that scattering of confined Dirac electrons in a narrow channel by an infinitely massive wall induces mode mixing, giving a qualitative reason for the fact that an analytical solution to the spectrum of Dirac electrons confined in a square box has not yet been found. A first attempt to solve this problem is presented. We find that only the trivial case $k = 0$ has a solution that does not require the existence of evanescent modes. We also study the spectrum of quantum dots of graphene in a perpendicular magnetic field. This problem is studied in the Dirac approximation, and its solution requires a numerical method whose details are given. The formation of Landau levels in the dot is discussed. The inclusion of the Coulomb interaction among the electrons is considered at the self-consistent Hartree level, taking into account the interaction with an image charge density necessary to keep the back-gate electrode at zero potential. The effect of a radial confining potential is discussed. The density of states of circular and hexagonal quantum dots, described by the full tight-binding model, is studied using the Lanczos algorithm. This is necessary to access the detailed shape of the density of states close to the Dirac point when one studies large systems. Our study reveals that zero-energy edge states are also present in graphene quantum dots. Our results are relevant for experimental research in graphene nanostructures. The style of writing is pedagogical, in the hope that newcomers to the subject will find this paper a good starting point for their research.

(Some figures in this article are in colour only in the electronic version)

1. Introduction

Graphene was discovered in 2004 at the Manchester Centre for Mesoscience and Nanotechnology, University of Manchester, UK, directed by Andre Geim [1, 2]. Previously, graphene was known only as an intrinsic part of three-dimensional systems: as individual atomic planes within graphite or its intercalated compounds and as the top few layers in epitaxially grown films [3]. In certain cases it was possible to even grow graphene monolayers on top of metallic substrates and silicon carbide [3]. However, coupling with the substrate did now allow studies of electronic, optical, mechanical, thermal and other properties of graphene, which all became possible after individual graphene layers were isolated. There are by now a number of review papers on graphene available in the literature, both qualitative [4–8] and quantitative [9, 10] in nature.

The original method of graphene isolation is based on micro-mechanical cleavage of a graphite surface—the so-called *Scotch Tape method*. This method, however, has a low yield of graphene micro-crystallites. Recently, a new method [12, 11], based on liquid-phase exfoliation of graphite, has proved to produce a large yield of graphene micro-crystallites, with large surface areas. A chemical approach to graphene production has also been achieved using exfoliation–reintercalation–expansion of graphite [13].

It is by now well known that graphene is a sheet of carbon atoms one atom thick, arranged in a honeycomb (hexagonal) lattice, having therefore two carbon atoms per

unit cell. The material can be considered the ultimate thin film. In a way, this material was the missing allotrope of pure carbon materials, after the discovery of graphite [14, 15], diamond [16], fullerenes and carbon nanotubes [14]. In fact we can think of graphene as being the raw material from which all other allotropes of carbon can be made [4, 5].

Although the Manchester team produced two-dimensional micro-crystallites of other materials [2], graphene attracted wide attention [17] from scientists due to its unexpected properties, associated with both fundamental and applied research.

Graphene has a number of fascinating properties. The stiffness of graphene has been proved to be so large, having a Young modulus $E \simeq 1.0$ TPa, that makes it the strongest material stiffness ever measured [11, 18]. In addition, the material has high thermal conductivity [19], is chemically stable and almost impermeable to gases [20], can withstand large current densities [1], has ballistic transport over sub-micron scales with very high mobilities in its suspended form ($\mu \simeq 200.000$ cm^2 V^{-1} s^{-1}) [1, 21, 22] and shows ambipolar behaviour [1]. Ballistic transport is in general associated with the observation of conductance quantization in narrow channels [23], which have recently been observed [24]. The above properties and its two-dimensional nature makes graphene a promising candidate for nano-electronic applications.

From the point of view of physical characterization we are interested in the mechanical properties of graphene, its electronic spectrum, its transport properties of heat, charge and spin, and its optical properties. The high stiffness of the material is responsible for the micro-crystallites keeping their planar form over time, without rolling up, even when graphene is held fixed by just one of its ends [11]. Interestingly, graphene is now being used, by combining electrostatic deposition methods and the chemical nature of the surrounding atmosphere, to produce rolled up nanotubes with controlled dimensions and chiralities [25]. The electronic spectrum of graphene and of graphene bilayers has been measured by angle resolved photoemission spectroscopy (ARPES) [26–29], fitting well with tight-binding calculations using a first nearest neighbour hopping $t \simeq 3$ eV and a second nearest neighbour hopping $t' \simeq 0.13$ eV [30].

The transport of heat has been measured experimentally and studied theoretically in a few papers [19, 31–34], and more research is needed to fully understand its properties, especially since the irradiation of graphene with laser light has been found to heat up the system locally [19]. The transport properties of graphene on top of silicon oxide have been extensively studied, but in a suspended geometry the few available experimental and theoretical studies are still recent [22, 35–37]. Of particular interest is the contribution of phonons to the transport properties of graphene. Although in the beginning of graphene research phonons were not considered to be important, recent experimental results show that this is, in fact, not the case [21, 38].

Of particular interest is the finite conductivity of graphene at the Dirac point, σ_D, the measured value of which is in contradiction to the naive single particle theory which predicts either infinite or zero resistance[3]. The value of σ_D is of the order of

$$\sigma_D \simeq \lambda 4 \frac{e^2}{h}, \tag{1}$$

with λ a number of order unity. We emphasize that equation (1) is the value for the conductivity of the material at the Dirac point, and not the conductance of a narrow channel. On the other hand, there is a discrepancy between the more elaborated theoretical descriptions of σ_D and the experimentally measured values, since the theory predicts the value $\sigma_D^{\text{theor.}} = \sigma_D/\pi$ [40–43], and most of the experiments measure a value given by equation (1). Adding to the problem, two experimental groups reported measurements of the conductivity of graphene consistent with the theoretical calculation [44, 45]. In this context it should be stressed that whereas the result of σ_D obtained in [40] comes about due to an increase of the density of states due to disorder (albeit small) at the Dirac point, the value for σ_D computed in [41, 42] is based on the existence of evanescent waves in clean graphene ribbons with large aspect ratio W/L (W is the width and L in the length of the ribbon). Recent experiments [44, 45] seem to confirm this latter view of the problem, since the value $\sigma_D^{\text{theor.}}$ is only measured in the regime $W/L \gg 1$. The transport of spin in graphene has been studied experimentally in few publications [46–49], and much work remains to be done.

The optical properties of graphene and of bilayer graphene have only recently been studied experimentally [50, 51], in contrast to the corresponding theoretical studies. The first theoretical study of graphene's optical absorption was made by Peres *et al* [40], followed by several studies by Gusynin *et al* and a review in [52]. The most relevant aspect was that the infrared conductivity of graphene, for photon energies larger than twice the chemical potential, has a universal value given by [40, 52, 37]

$$\sigma_0 = \frac{\pi}{2}\frac{e^2}{h}. \tag{2}$$

Theoretical studies preceded experimental measurements for the bilayer as well [55–57]. Due to the existence of four energy bands in bilayer graphene, its optical spectrum has more structure than the corresponding single layer one.

It was experimentally found that for photon energies in the visible range [53] equation (2) also holds within less than 10% difference [54]. This result makes graphene the first conductor with light transmissivity in the frequency range from infrared to the ultraviolet as high as

$$T \simeq 1 - \pi\alpha \sim 98\%, \tag{3}$$

with α the fine structure constant. This makes it obvious that graphene can be used as a transparent metallic electrode, having found applications in solar cell prototypes [58, 59] and in gateable displays [60]. The same conclusions are obtained from studying the optical conductivity of graphite [61]. The

[3] The *naive single particle theory* is related to the semi-metallic nature of the spectrum of graphene. The absence of a gap would suggest an infinite conductivity; the zero density of states at the Dirac point would suggest zero conductivity. The fact is that in the clean case the DC conductivity is finite at zero temperature and zero at finite temperature [39].

transparency of graphene has an obvious advantage over the more traditional materials used in the solar cell industry, namely indium tin oxide (ITO) and fluorine tin oxide (FTO), which have a very low light transmission for wavelengths smaller than 1500 nm; in the visible range the transparency of these two materials is larger than ∼85%. Furthermore, these traditional materials have a set of additional problems [58, 60], such as chemical instability, which are not shared by graphene. On the other hand, ITO and FTO have a low resistivity (∼5 Ω m), a figure that graphene cannot match, if one leaves aside the possibility of graphene film deposit from solution.

Finally, the interaction of graphene with single molecules allows graphene to be used as a detector of tiny numbers of molecules [62] and to enhance, in a dramatic way, the sensibility of ordinary transmission electron microscopes [12, 63], allowing the observation of adsorbates, such as atomic hydrogen and oxygen, which can be seen as if they were suspended in free space.

Many of the above properties are expected to be present in graphene nanoribbons. On the other hand, aspects related to the quantum confinement of electrons in graphene, both considering confinement in one (quantum wire) or two (quantum dot) dimensions, is expected to bring new interesting phenomena. The present state of the art of material manipulation technologies does not allow the production structures, in a top-down approach, smaller than 10 nm. Nevertheless, many aspects associated with the quantum confinement of electrons in graphene, either due to narrow constrictions or due to the formation of quantum dots, have already been investigated experimentally [64–68] and theoretically [69–77]. One important consequence of quantum confinement is the appearance of an energy gap in the electronic spectrum of graphene, an important characteristic if graphene is to be used as a material to build nano-transistors [79]. In this paper we will address several properties of confined Dirac electrons by considering both nano-wires and quantum dots of graphene. In doing this we use both the continuous Dirac approximation and the tight-binding description, choosing whichever one is more appropriate for the given problem.

In this paper we will address several properties of confined Dirac electrons by considering both nano-wires and quantum dots of graphene, both using the continuous Dirac approximation and the tight-binding model. We start by discussing the confinement of massless Dirac fermions, stating that such cannot be achieved by electrostatic potentials due to Klein tunnelling [10]. One possible way out is to change locally the spectrum from the massless to massive case and taking the limit $M \to \infty$ at the end of the calculation. This type of boundary condition is termed an infinite mass boundary condition. Other possibility is the use of boundary conditions derived from the tight-binding solution [80]. The differences between the two approaches occur only for mini-bands close to the Dirac point, where the slightly different quantization rule of the momentum leads to slightly different values of the energy spectrum. For those cases where the length of the ribbon is much larger then the lattice spacing there is almost no difference between the two approaches. Another difference between the two types of boundary condition lies in the fact that for zigzag nanoribbons there are surface states and for armchair nanoribbons there are metallic states for some particular values of the ribbon width; for the infinite mass boundary condition both these two possibilities are absent. Nevertheless, from the experimental point of view [24, 79] the nanoribbons do not have a well-defined edge structure—they are not either pure zigzag or pure armchair. As a consequence, the ribbons patterned from graphene crystallites are found to have a finite energy gap [24, 79]. Therefore, our use of the infinite mass boundary condition is experimentally justified and can be thought of as a phenomenological model for the one-dimensional bands present in the nanoribbons (see equation (1) of [24]). Of particular interest is our result of the what happens when a Dirac electrons is reflected back at the end of a semi-infinite graphene nanoribbon. Contrary to the Schrödinger case, mode mixing takes place in this scattering event, which is a consequence of the confinement in the transverse direction and the spinorial nature of the wavefunction. One aspect we do not address in our paper is the formation of energy gaps in zigzag nanoribbons due to the formation of magnetic states at the edges of the ribbon [81] and also proposed for the bilayer case [82].

If graphene is patterned in such a way that confinement is induced in wo dimensions, one enters the realm of artificial atoms or graphene quantum dots. As we have mentioned above, there is already some literature available on graphene quantum dots [69–77], but these studies have not address the effect of electron–electron interactions in the dot when the system is gated away from the Dirac point and how these interactions change the single particle energy levels of the system. Of special interest is the interference of electrons in graphene rings [73], an aspect that is not covered in our paper. In this paper we study the effect of electron–electron interactions at the Hartree level. Quantum dots have been studied either using the effective Dirac Hamiltonian [76, 78], with an additional central potential, or using the natural boundary conditions introduced by the tight-binding Hamiltonian [77]. In our study we introduce both the boundary condition implied by the tight-binding model [80] and another extra central potential energy which represents both the effect of the etching and of the gates, together with electron–electron interaction. This additional potential is treated exactly using a numerical model developed specifically for this problem. We found that in this case the energy levels vary in energy with the angular momentum quantum number. Our studies therefore extend previous ones on graphene quantum dots.

2. The tight-binding model and the Dirac approximation

The experimental work cited in section 1 constitutes a vast body of evidence that the low energy theory of electrons in graphene is described by the two-dimensional Dirac equation, which is obtained as an $\boldsymbol{k} \cdot \boldsymbol{p}$ expansion around the Dirac points in momentum space [9, 83]. In figure 1 we represent a finite-size ribbon of a hexagonal lattice. Two features are of

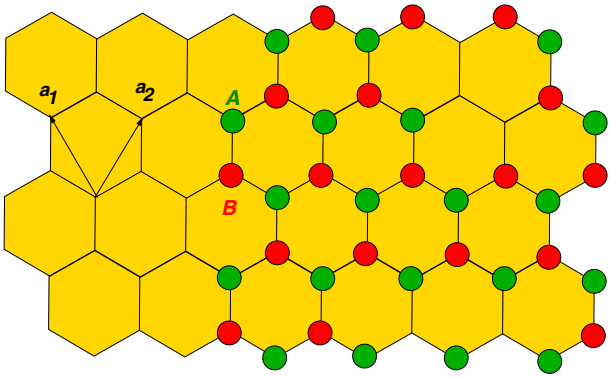

Figure 1. A honeycomb ribbon, with zigzag edges (top and bottom) and armchair edges (vertical ones), with the carbon atoms belonging to the sub-lattices A and B clearly differentiated from each other (with several carbon atoms represented). The lattice unit vectors $\boldsymbol{a}_1$ and $\boldsymbol{a}_2$ are also shown.

importance: the first is that the lattice is not a Bravais lattice, being instead made of two inter-penetrating triangular lattices, giving rise to two geometrically non-equivalent carbon atoms, termed A and B; the second is that there are two different types of edges present—zigzag and armchair edges. These types of edge play a different role in the physics of the ribbon. In particular, note that the zigzag edges are made up of a single type of atom, B on top and A at the bottom (in the case of this figure). As is shown in figure 1, we can choose the direct lattice vectors to be the following:

$$\boldsymbol{a}_1 = \frac{a}{2}(-1, \sqrt{3}), \tag{4}$$

$$\boldsymbol{a}_2 = \frac{a}{2}(1, \sqrt{3}), \tag{5}$$

where $a = 2.46$ Å is the lattice vector length. As a consequence, the reciprocal lattice vectors are

$$\boldsymbol{b}_1 = \frac{2\pi}{a}\left(-1, \frac{1}{\sqrt{3}}\right), \tag{6}$$

$$\boldsymbol{b}_2 = \frac{2\pi}{a}\left(1, \frac{1}{\sqrt{3}}\right). \tag{7}$$

The so-called Dirac points in the honeycomb Brillouin zone are conveniently chosen to be

$$\boldsymbol{K} = \frac{4\pi}{3a}(1, 0), \tag{8}$$

$$\boldsymbol{K}' = \frac{4\pi}{3a}(-1, 0). \tag{9}$$

If one considers only the hopping process t (first nearest neighbour hopping), the tight-binding Hamiltonian is very easily written as (N_c is the number of unit cells in the solid)

$$H = -t\sum_{i,\boldsymbol{\delta},\sigma}^{N_c}(a^\dagger_{i,\sigma}b_{i+\boldsymbol{\delta},\sigma} + \text{h.c.}), \tag{10}$$

where $a^\dagger_{i,\sigma}$ creates an electron with spin projection σ in the π-orbital of the carbon atom of the sub-lattice A, and of the unit cell i; a similar definition holds for $b^\dagger_{i,\sigma}$. N_c is the number of unit cells in the crystal and $\boldsymbol{\delta}$ represents the three vectors connecting the three first neighbours of the carbon atom A. The exact diagonalization of this problem is straightforward, leading to

$$E_\pm = \pm t\sqrt{3 + 2\cos(ak_x) + 4\cos\left(\frac{a}{2}k_x\right)\cos\left(\frac{a\sqrt{3}}{2}k_y\right)}.$$

We can expand this relation near the Dirac points, obtaining ($\boldsymbol{k} = \boldsymbol{q} + \boldsymbol{K}$)

$$E_\pm \simeq \pm v_F|\vec{q}|, \tag{11}$$

which is a massless Dirac-like linear dispersion relation, where the velocity of light is substituted by $v_F = \frac{a\sqrt{3}}{2\hbar}t \simeq 10^6$ m s^{-1}, the Fermi velocity. To obtain the effective Hamiltonian obeyed by the electrons near the Dirac points we write the matrix Hamiltonian in momentum space as

$$H_{\boldsymbol{k}} = -t\begin{pmatrix} 0 & s_{\boldsymbol{k}} \\ s^*_{\boldsymbol{k}} & 0 \end{pmatrix}, \tag{12}$$

with $s_{\boldsymbol{k}}$ given by ($\boldsymbol{k} = \boldsymbol{q} + \boldsymbol{K}$)

$$\begin{aligned} s_{\boldsymbol{k}} &= 1 + \mathrm{e}^{\mathrm{i}\boldsymbol{K}\cdot\boldsymbol{a}_1}\,\mathrm{e}^{\mathrm{i}\boldsymbol{q}\cdot\boldsymbol{a}_1} + \mathrm{e}^{\mathrm{i}\boldsymbol{K}\cdot\boldsymbol{a}_2}\,\mathrm{e}^{\mathrm{i}\boldsymbol{q}\cdot\boldsymbol{a}_2} \\ &\simeq -\frac{a\sqrt{3}}{2}(q_x + \mathrm{i}q_y), \end{aligned}$$

leading to the effective Hamiltonian (one valid near $\boldsymbol{K}$ and the other near $\boldsymbol{K}'$)

$$H_{\boldsymbol{K}}(\boldsymbol{q}) = v_F\boldsymbol{\sigma}^*\cdot\boldsymbol{q} \tag{13}$$

$$H_{\boldsymbol{K}'}(\boldsymbol{q}) = v_F\boldsymbol{\sigma}\cdot\boldsymbol{q}, \tag{14}$$

with $\boldsymbol{\sigma} = (\sigma_x, \sigma_y)$ and $\boldsymbol{\sigma}^* = (\sigma_x, -\sigma_y)$. The Hamiltonian (13), or alternatively (14), will be the starting point of our discussion.

Let us assume that it is possible to create a potential such that a term of the form

$$V = \sum_{i,\sigma}^{N_c} v_F^2 m(a^\dagger_{i,\sigma}a_{i,\sigma} - b^\dagger_{i,\sigma}b_{i,\sigma}), \tag{15}$$

is added to the Hamiltonian (10). In terms of the formalism used to write the effective Hamiltonian (13) and (14), this term is rewritten as

$$V = v_F^2 m\sigma_z, \tag{16}$$

and it corresponds to the presence of a mass term in the Hamiltonian. This type of term can be generated by covering the surface of graphene with gas molecules [84] or by depositing graphene on top of boron nitride [85–87]. The eigenvalues of $H_{\boldsymbol{K}} + V$ are easily obtained, leading to $E = \pm\sqrt{v_F^2\hbar^2|k|^2 + m^2v_F^4}$, with $|k| = \sqrt{k_x^2 + k_y^2}$, and the same for $H_{\boldsymbol{K}'} + V$.

3. Confinement of Dirac electrons on a strip

Our goal in this section is to derive a mathematical framework for describing the effect of confinement on Dirac electrons. The confinement can be produced either by etching, by the reduced dimensions of the graphene crystallites or by the application of gate potentials (here Klein tunnelling poses strong limitations on the use of such a method).

3.1. Boundary conditions and transverse momentum quantization

The mathematical description of the confinement requires the imposition of appropriate boundary conditions to the Dirac fermions. Although, for graphene ribbons, the two types of edges discussed above impose two different types of boundary conditions [80], we shall use here the infinite mass confinement[4] proposed by Berry and Mondragon [91]. For large ribbons, there will be no important difference between the two types of boundary condition [92], except that the infinite mass boundary condition is not able to produce edge states [93], which are present in ribbons with zigzag edges.

We shall generalize some of the results of [41, 91] by considering the case of Dirac fermions with a finite mass. The mass profile in the transverse direction (y) of the strip is represented in figure 2. The boundary conditions that the wavefunction has to obey, at the spatial point where the mass changes from m to M, are derived considering the reflection of the wavefunction at the boundary. Let us first consider the reflection at $y = L/2$. The wavefunction in the central region (I) is given by

$$\psi_{\rm I}(x, y) = \left[\begin{pmatrix} 1 \\ f_{\rm I}(E)\, {\rm e}^{{\rm i}\theta_k} \end{pmatrix} {\rm e}^{{\rm i}k_y y} + R \begin{pmatrix} {\rm e}^{{\rm i}\theta_k} f_{\rm I}(E)^{-1} \\ 1 \end{pmatrix} {\rm e}^{-{\rm i}k_y y}\right] {\rm e}^{{\rm i}k_x x}, \tag{17}$$

with $\theta_k = \arctan(k_y/k_x)$,

$$f_{\rm I}(E) = \frac{E - m v_{\rm F}^2}{\sqrt{E^2 - m^2 v_{\rm F}^4}}. \tag{18}$$

In zone II ($y > L/2$), the solution has the form

$$\psi_{\rm II}(x, y) = T \begin{pmatrix} 1 \\ f_{\rm II}(E) \end{pmatrix} {\rm e}^{{\rm i}q_y y}\, {\rm e}^{{\rm i}k_x x}, \tag{19}$$

with

$$f_{\rm II}(E) = \frac{E - M v_{\rm F}^2}{v_{\rm F}\hbar(k_x - {\rm i}q_y)}, \tag{20}$$

and

$$q_y = \pm\sqrt{\frac{E^2 - M^2 v_{\rm F}^4}{v_{\rm F}^2\hbar^2} - k_x^2}, \tag{21}$$

[4] It is important to comment here on this particular choice for the boundary condition. Using the $\boldsymbol{k}\cdot\boldsymbol{p}$ approach of DiVincenzo and Mele [83] one learns that $v_{\rm F} \propto 1/m$, where m is the bare electron mass. On the other hand, one considers that graphene electrons cannot propagate in a region where the material is absent, and therefore have zero velocity there. Due to the proportionality $v_{\rm F} \propto 1/m$ this can be achieved taking the limit $m \to \infty$. Therefore we could think that confinement of Dirac fermions could be achieved with a position dependent Fermi velocity $v_{\rm F}(y)$ that goes to zero at the edge of the strip. Unfortunately this program does not work. The Berry and Mondragon boundary condition [91] corresponds to a change in the nature of the spectrum, and is somewhat artificial concerning graphene. The consequences of the different boundary conditions are: the properties of the wavefunction at the graphene edges do depend on the different choices of boundary conditions, but the bulk behaviour of the electronic states is essentially the same for all them; very close to the neutrality point the choice of boundary conditions does again matter, but at finite doping this is no longer the case. The choice of the Berry and Mondragon boundary condition [91] does introduce a certain degree of simplicity to the calculations.

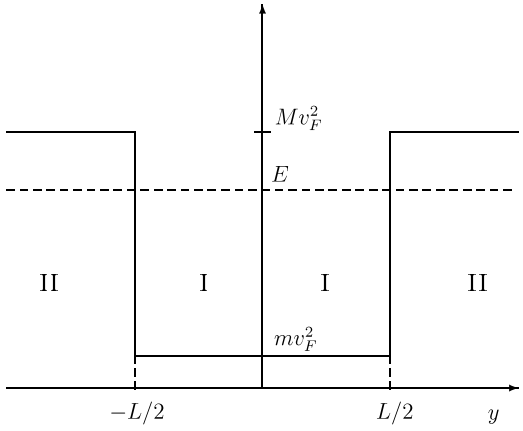

Figure 2. Scheme of the mass confinement (along y) with mass m inside the strip and mass M outside. The dashed line represents the energy of the electron.

where the energy values are given by the same expression as that for zone I. As we want to take the limit $M \to \infty$, we will assume $M v_{\rm F}^2 > E$, which implies that

$$q_y = \pm{\rm i}\sqrt{\frac{M^2 v_{\rm F}^4 - E^2}{v_{\rm F}^2\hbar^2} + k_x^2} = \pm{\rm i}|q_y|, \tag{22}$$

and thus

$$f_{\rm II}(E) = \frac{E - M v_{\rm F}^2}{v_{\rm F}\hbar(k_x + |q_y|)} = \frac{E - M v_{\rm F}^2}{v_{\rm F}\hbar\left(k_x \pm \sqrt{\frac{M^2 v_{\rm F}^4 - E^2}{v_{\rm F}^2\hbar^2} + k_x^2}\right)}, \tag{23}$$

where the sign $\pm$ in front of the square root applies to the wavefunction that is propagating in the positive/negative y direction. Imposing the boundary condition associated with the Dirac equation for a reflection at $y = L/2$,

$$\psi_{\rm I}\left(x, \frac{L}{2}\right) = \psi_{\rm II}\left(x, \frac{L}{2}\right), \tag{24}$$

one obtains

$$\frac{\psi_{{\rm I}_1}}{\psi_{{\rm I}_2}} = \frac{\psi_{{\rm II}_1}}{\psi_{{\rm II}_2}} = \frac{1}{f_{\rm II}(E)}. \tag{25}$$

Taking the limit $M \to \infty$ the boundary conditions reduce to

$$\left.\frac{\psi_{{\rm I}_1}}{\psi_{{\rm I}_2}}\right|_{y=-L/2} = +1, \tag{26}$$

$$\left.\frac{\psi_{{\rm I}_1}}{\psi_{{\rm I}_2}}\right|_{y=L/2} = -1. \tag{27}$$

Now one wants to write down the wavefunction of electrons propagating on the strip taking into account the confinement due to the mass term. The most general wavefunction is of the sum of two counter-propagating waves in the y direction

$$\psi(x, y) = \chi(y)\, {\rm e}^{{\rm i}k_x x}, \tag{28}$$

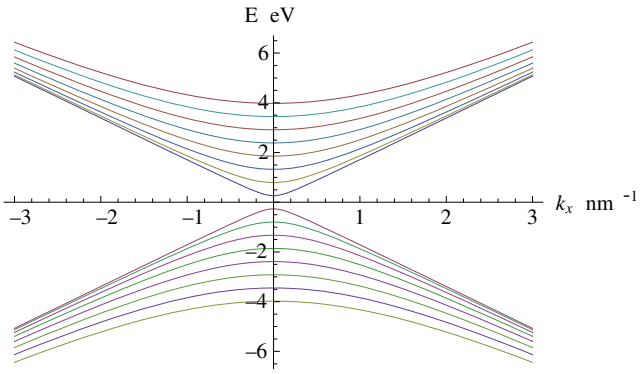

Figure 3. Energy levels of a ribbon 10 nm wide. The transverse modes range from $n = 0$ to 8, for both particles and holes.

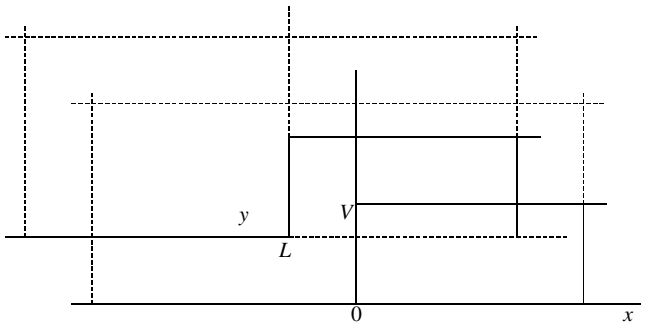

Figure 4. Representation of a step potential in a strip with lateral confining infinite mass. Zone I is for $x < 0$ and zone II is for $x > 0$. The dashed lines represent the confinement of the electrons.

where

$$\chi(y) = A \begin{pmatrix} 1 \\ f_1(E)\, e^{i\theta_k} \end{pmatrix} e^{ik_y y} + B \begin{pmatrix} 1 \\ f_1(E)\, e^{-i\theta_k} \end{pmatrix} e^{-ik_y y}. \tag{29}$$

It is always possible to redefine B such that

$$\chi(y) = A \begin{pmatrix} 1 \\ f_1(E)\, e^{i\theta_k} \end{pmatrix} e^{ik_y y} + B \begin{pmatrix} e^{i\theta_k} f_1(E)^{-1} \\ 1 \end{pmatrix} e^{-ik_y y}, \tag{30}$$

a procedure that proves useful later on. Imposing the boundary conditions (27), one obtains (considering the strip to be in the range $0 < y < L$ for simplicity)

$$B = \frac{1 - f_1(E)\, e^{i\theta_k}}{1 - f_1(E)^{-1} e^{i\theta_k}} A, \tag{31}$$

for the relation between the coefficients, and

$$e^{ik_y L} = -\frac{1 - f_1(E)\, e^{i\theta_k}}{1 - f_1(E)^{-1} e^{i\theta_k}} \frac{1 + f_1(E)^{-1} e^{i\theta_k}}{1 + f_1(E)\, e^{i\theta_k}} \tag{32}$$

for the energy quantization. It is clear that the admissible values of k_y are energy dependent. Considering the limit $M \to \infty$ one obtains, from equation (31), the simpler result $A = B$, and, from equation (32), the condition $e^{i2k_y L} = -1$, which leads to the transverse momentum quantization rule [91]

$$k_{y_n} = \frac{\pi}{2L} + \frac{n\pi}{L}, \qquad \text{where } n = 0, \pm 1, \pm 2, \ldots. \tag{33}$$

The result for momentum quantization in equation (33) is quite similar to that found for nanoribbons with armchair edges[5]. Putting all this together, the obtained results are summarized as:

$$\begin{aligned} \psi_{n,k}(x, y) &= \chi_{n,k}(y)\, e^{ikx}, \\ \chi_{n,k}(y) &= A \left[\begin{pmatrix} 1 \\ z_{n,k} \end{pmatrix} e^{iq_n y} + \begin{pmatrix} z_{n,k} \\ 1 \end{pmatrix} e^{-iq_n y} \right], \end{aligned} \tag{34}$$

where we have used $k = k_x$, $q_n = k_{y_n}$, $s = \pm 1 = \mathrm{sgn}[E]$ and

$$z_{n,k} = s\, e^{i\theta_k} = s \frac{k + iq_n}{\sqrt{k^2 + q_n^2}}.$$

[5] From [80] the momentum quantization for nanoribbons with armchair edges has the form $k_n = n\pi/(L + a/2) + 2\pi/(3a)$. The constant term in k_n implies that the system has an energy gap.

If we ignore questions of convergence, we recognize that this form for $z_{n,k}$ does not require k or q_n to be real. We are only assuming $k^2 + q_n^2 > 0$. The dependence of the energy E on k shows a number of sub-bands separated by energy gaps; this is shown in figure 3 for a ribbon 10 nm wide. It is clear that for such a narrow ribbon one has large energy gaps between two consecutive sub-bands.

Let us represent equation (34) as $|\Psi_{n,k}\rangle = |\chi_{n,k}\rangle\, e^{ikx}$, it is then simple to show that $\langle \Psi_{m,k'} | \Psi_{n,k} \rangle = 0$ and that the normalization coefficient A reads $A = 1/(2\sqrt{L})$. Note that if on the strip we have a non-zero scalar potential $\hat{1}V$, we will just have to substitute E by $E - V$ and replace k by $\tilde{k}$, with $\tilde{k}$ given by

$$\tilde{k}^2 = \frac{(E - V)^2}{v_F^2 \hbar^2} - \frac{v_F^2 m^2}{\hbar^2} - q_n^2. \tag{35}$$

3.2. Dirac fermions in a strip with a step potential

Let us now consider the scattering of Dirac fermions in a strip by a simple step potential, as represented in figure 4. In zone I one has $V = 0$, the wavefunction is given by equation (34); in zone II, with $V > 0$, the wavefunction is also given by equation (34) making the replacement $k \to \tilde{k}$. If, in general, the step rises up at $x = X$ the boundary condition takes the form

$$\psi_{n,k}(X, y) + r_n \psi_{n,-k}(X, y) = t_n \psi_{n,\tilde{k}}(X, y). \tag{36}$$

Solving for r and t gives

$$r_n = \frac{z_{n,k}^2 - z_{n,k} z_{n,\tilde{k}}}{1 + z_{n,k} z_{n,\tilde{k}}}\, e^{2ikX}, \tag{37}$$

$$t_n = \frac{1 + z_{n,k}^2}{1 + z_{n,k} z_{n,\tilde{k}}}\, e^{-i(\tilde{k} - k)X}. \tag{38}$$

Equations (37) and (38) represent the reflection and the transmission amplitudes, respectively, for the transverse mode n. It is now a simple matter to compute the tunnelling transmission for an arbitrary configuration of finite potential steps by using these two results combined with a transfer matrix method [87]. A particular case of this situation is transmission through a potential barrier, for which $|t_n|^2$ is given in figure 5.

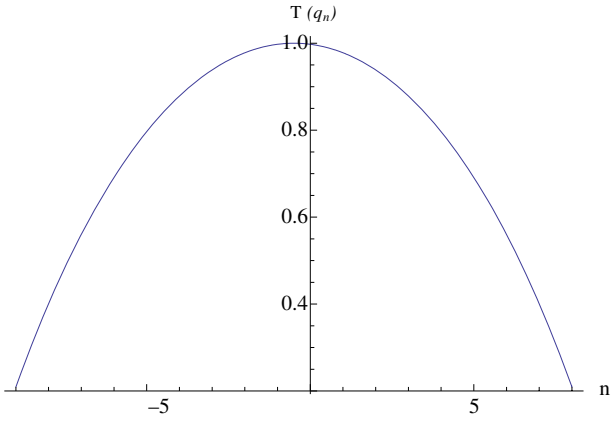

Figure 5. Transmission coefficient, $T(q_n) = |t_n|^2$, through an energy barrier of length $w = 100$ nm and height $V = 50$ eV as a function of the transverse quantization quantum number n. The energy of the electron is taken as $E = 0.1$ eV and the width of the ribbon is $L = 500$ nm.

3.3. Trapped eigenmodes

In this section we will show that it is possible to trap massless Dirac electrons in a ribbon of finite width L by creating a p–n–p junction [88, 90]. The effect exploits the fact that the spectrum of a finite ribbon exhibits energy gaps. A similar study was done in [94] for the bulk case. In this case, such a confinement is possible for certain incident angles of the eigenmodes on the potential walls [94]. The potential profile considered is shown in figure 6. We show that the trapping of the eigenmodes requires evanescent modes in the x direction. This can be accomplished using a scalar potential.

In order to solve this problem let as again consider the case of a potential step as in figure 6. In region I ($x < w$) the wavefunction has the form (34) and in region II ($x > w$) the form would be the same with k replaced by

$$\tilde{k} = \sqrt{\left(\frac{E-V}{v_F\hbar}\right)^2 - q_n^2}. \tag{39}$$

One now makes the observation that if q_n obeys the condition

$$\frac{(E-V)^2}{v_F^2\hbar^2} < q_n^2 < \frac{E^2}{v_F^2\hbar^2}, \tag{40}$$

one has a propagating wave in region I and an evanescent wave in region II. Within the validity of equation (40) it is more transparent to write the wavefunction in region II as

$$\psi_{\mathrm{II}_{n,\tilde{k}}}(x,y) = \frac{1}{2\sqrt{L}}\left[\begin{pmatrix} 1 \\ \mathrm{i}s'\frac{\alpha+q_n}{\sqrt{q_n^2-\alpha^2}} \end{pmatrix} \mathrm{e}^{\mathrm{i}q_n y} + \begin{pmatrix} \mathrm{i}s'\frac{\alpha+q_n}{\sqrt{q_n^2-\alpha^2}} \\ 1 \end{pmatrix} \mathrm{e}^{-\mathrm{i}q_n y}\right] \mathrm{e}^{-\alpha x}, \tag{41}$$

with

$$\tilde{k} = \mathrm{i}\alpha = \mathrm{i}\sqrt{q_n^2 - \left(\frac{E-V}{v_F\hbar}\right)^2}, \tag{42}$$

where $s' = \mathrm{sgn}[E-V]$. Of course, the same type of analysis would hold if one considered the step at $x = 0$, starting at the interface between regions III and I. The trapping 'mechanism' uses this fact. The wavefunction in region I of figure 6 is taken as a sum of two counter-propagating waves along the x direction, whereas in regions II and III only evanescent waves exist. Imposing the boundary conditions at $x = 0$ and w (w the width of the well) one obtains after a lengthy calculation the condition of the energy of the trapped eigenmodes

$$\sin(kw)F(E,V,q_n) + \cos(kw)G(E,V,q_n) = 0, \tag{43}$$

with

$$F(E,V,q_n) = \frac{\mathrm{i}}{16}[-4(z_{n,k}^* + z_{n,k})^2 - (z_{n,k} - z_{n,k}^*)(z_{n,\alpha} + z_{n,-\alpha}) - (z_{n,k}^3 - (z_{n,k}^*)^3)(z_{n,\alpha} + z_{n,-\alpha})], \tag{44}$$

and

$$G(E,V,q_n) = \tfrac{3}{16}(z_{n,k} + z_{n,k}^* + z_{n,k}^3 + (z_{n,k}^*)^3)(z_{n,\alpha} - z_{n,-\alpha}). \tag{45}$$

Both $F(E,V,q_n)$ and $G(E,V,q_n)$ are pure imaginary numbers, as long as condition (40) holds true. In order to give a flavour of the numerical solution of equation (43) we present its numerical solution in table 1. We have chosen the strategy of fixing the energy and looking for the values of w that satisfy equation (43), for different values of q_n.

4. Inducing mode mixing by scattering at a wall

In this section we want to discuss the scattering of Dirac electrons when they propagate along a semi-infinite narrow

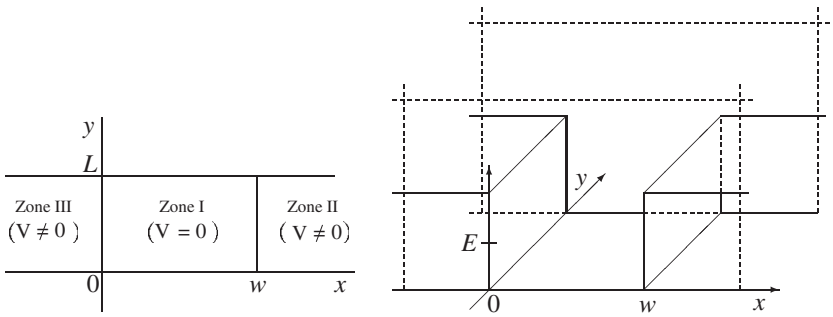

Figure 6. Scheme of the confinement (along y) in a strip where a scalar potential well, of width w, was created. On the left one has an upper view and on the right one has a side view. The dashed lines represent the confinement of the electrons.

Table 1. Values of w (in nm) for a given momentum q_n (in nm^{-1}). The parameters are $s = 1$, $s' = -1$, $v_F = 10^6$ m s^{-1}, $E = 0.1$ eV, $V = 0.15$ eV and $L = 500$ nm.

n	w	n	w	n	w	n	w
5	∼59	6	∼65	7	∼78	8	∼113

channel and scatter back at the wall located at the end of the channel. This problem is intimately related to the possibility of finding a solution for the eigenmodes and eigenstates of trapped Dirac electrons in a square box. Our analysis hints at the reason why this solution has not been found yet.

4.1. Definition of the problem

Let us now consider massless Dirac fermions confined in a semi-infinite strip: $x < 0$ and $0 < y < L$. We will look for scattering states produced by the scattering at the wall due to an incoming wave from $x \to -\infty$. As before, the fermions are confined by an infinite mass term outside the strip.

The scattering state is a sum of an incoming wave, with energy E, longitudinal momentum k and transverse momentum q_n, with a superposition of all the possible outgoing channels with reflection amplitude $r_{n,m}$, and it can be written as

$$\begin{aligned}\Psi_{n,k}(x,y) &= \begin{pmatrix}\Psi_1(x,y)\\ \Psi_2(x,y)\end{pmatrix}\\ &= \left[\begin{pmatrix}1\\ z_{n,k}\end{pmatrix} e^{iq_n y} + \begin{pmatrix}z_{n,k}\\ 1\end{pmatrix} e^{-iq_n y}\right] e^{ikx}\\ &\quad + \sum_{m=0}^{\infty} r_{n,m}\left[\begin{pmatrix}1\\ z_{m,-k_m}\end{pmatrix} e^{iq_m y} + \begin{pmatrix}z_{m,-k_m}\\ 1\end{pmatrix} e^{-iq_m y}\right]\\ &\quad \times e^{-ik_m x}. \end{aligned} \tag{46}$$

Since we are considering elastic scattering (Ψ is an eigenstate), we must have

$$E^2 = k_m^2 + q_m^2 = k^2 + q_n^2,$$

i.e.,

$$k_m^2 = k^2 + q_n^2 - q_m^2. \tag{47}$$

We must distinguish two situations:

$$q_m^2 < E^2 \Rightarrow k_m = \sqrt{E^2 - q_m^2}, \tag{48}$$

$$q_m^2 > E^2 \Rightarrow k_m = i\sqrt{q_m^2 - E^2}. \tag{49}$$

The second case corresponds to evanescent modes. We must choose this solution if we want the wavefunction to be convergent for $x \to -\infty$; for real k_m the choice of sign reflects the fact that we have only one incoming mode. We now simplify the notation, using the fact that k and n are fixed, and define

$$z_{n,k} = \frac{k + iq_n}{s\sqrt{k^2 + q_n^2}} = z_n, \tag{50}$$

$$z_{m,-k_m} = \frac{-k_m + iq_m}{s\sqrt{k^2 + q_m^2}} = \tilde{z}_m. \tag{51}$$

The parameter z_n is just a phase, $|z_n|^2 = 1$; $\tilde{z}_m$ is also a phase for propagating modes, but for evanescent modes $|\tilde{z}_m|^2 \neq 1$. For $q_m^2 \gg E^2$, we obtain

$$\tilde{z}_m \approx \frac{-iq_m(1 - E^2/2q_m^2) + iq_m}{E} \approx i\frac{E}{2q_m^2} \to 0.$$

4.2. Calculation of the reflection coefficients

The boundary condition at the end of the semi-infinite strip $x = 0$ and $0 < y < L$ is (see section 5 for details)

$$\Psi_1(0, y) + i\Psi_2(0, y) = 0. \tag{52}$$

Note that the boundary condition at an infinite mass vertical wall is different from that of the horizontal case discussed before. Applying the boundary condition (52) to $\Psi_{n,k}(x, y)$ and after rather lengthy algebra (where the replacement $-(m+1) = m'$ is made at some stage and m' is redefined as m afterwards) one arrives at the condition

$$\sum_{m=-\infty}^{\infty} I(n, m)\, e^{iq_m y} = 0, \tag{53}$$

with $I(n, m)$ given by

$$\begin{aligned} I(n,m) &\equiv \left[(1 + iz_m)\,\delta_{n,m} + r_{n,m}(1 + i\tilde{z}_m)\right]\theta(m + 1/2)\\ &\quad + \left[(z_{-m-1} + i)\,\delta_{n,-m-1} + r_{n,-m-1}(\tilde{z}_{-m-1} + i)\right]\\ &\quad \times \theta(-1/2 - m). \end{aligned} \tag{54}$$

The crucial step in the derivation is the observation that the set of functions $\{\phi_m = e^{iq_m y}, m = 0, \pm1, \pm2, \ldots\}$ is *overcomplete*. In fact, the set of states with m even (or with m odd) is, by itself, a complete orthogonal set for functions defined in the interval $0 < y < L$. If follows that we obtain an equivalent set of conditions to equation (53) by taking inner products of equation (53) with ϕ_m with m even (or m odd). We recall the inner products (choosing p even) to be

$$\begin{aligned} &\frac{1}{L}\int_0^L dy\, e^{-i(q_p - q_m)y}\\ &= \begin{cases} 1, & p = m\\ 0, & m \text{ is even}, m \neq p\\ \dfrac{2}{i(p-m)\pi}, & m \text{ is odd.}\end{cases} \end{aligned} \tag{55}$$

The fact that the integral (55) is not a Kronecker symbol shows that, in this case, the basis is overcomplete. Using equation (55), we obtain

$$\begin{aligned} &I(n, p) + \sum_{m_{\text{odd}}} \frac{2}{i(p-m)\pi} I(n, m) = 0\\ &\qquad p = 0, \pm2, \pm4, \ldots \end{aligned} \tag{56}$$

which is the central result of this section. This is the set of equations needed to calculate the $r_{n,m}$ coefficients. Naturally the convergence of the sum in (56) critically depends on the behaviour of $r_{n,m}$ with m.

We could also have formulated the scattering problem a bit more generally, considering, for example, the case of

a wave that approaches a wall at $x = -D$ coming from $x = +\infty$. Naturally the modifications relative to the solution found before cannot be extensive, given the symmetry of the problem. The first thing to note is that the boundary condition is slightly changed, being given by (see section 5 for details)

$$\Psi_1(-D, y) - \mathrm{i}\Psi_2(-D, y) = 0. \tag{57}$$

Working out the problem along the same lines as before, one learns that the final result can be obtained from the previous solution upon the replacements

$$r_{n,m} \to r_{n,m}\, \mathrm{e}^{\mathrm{i}D(k+k_m)}, \tag{58}$$

$$z_m \to -1/z_m, \tag{59}$$

$$\tilde{z}_m \to -1/\tilde{z}_m, \tag{60}$$

where the transformation (58) is obtained using the generator of translations, $\hat{T}(x_0) = \mathrm{e}^{\mathrm{i}x_0\hat{p}/\hbar}$ (with $\hat{p}$ the momentum operator), and follows from the new position of the wall. The transformations (59) and (60) follow from the difference in the boundary condition between a right and a left vertical wall. One should note that the transformation (58) is not a phase for evanescent waves. Using transformations (58)–(60) in equation (54) one obtains

$$\begin{aligned} I(n, m) \to\ & [(1 + \mathrm{i}/z_m)\delta_{n,m} + \mathrm{e}^{\mathrm{i}D(k+k_m)} r_{n,m}(1 + \mathrm{i}/\tilde{z}_m)] \\ & \times \theta(m + 1/2) - [(1/z_{-m-1} + \mathrm{i})\, \delta_{n,-m-1} \\ & + \mathrm{e}^{\mathrm{i}D(k+k_{-m-1})} r_{n,-m-1}(1/\tilde{z}_{-m-1} + \mathrm{i})]\theta(-1/2 - m). \end{aligned} \tag{61}$$

Naturally, the exact solution of the scattering problem rests upon the possibility of solving exactly the set of linear equations (56). This task seems out of reach at the moment. The second approach is to solve this set of equations numerically. This leads to the conclusion that the summation over m has to be truncated at some value. To be concrete, let us consider the particular case of an incoming mode with transverse quantum number $n = 0$, such that the value of the incoming longitudinal momentum k originates N_p propagating modes above the mode $n = 0$ ($0 < N_p < N$). Then the numerical solution of the problem has to satisfy the conservation of the probability density current (it must be 1 in this case) and the retained coefficients after the truncation have to converge upon increasing N. As we show below, both these two conditions are satisfied for small N. For the numerical solution we choose $n = 0$, $q_0 = \pi/2$, such that the value of $k = 2\pi$ leads to $n = 0$ and 1 as the only two propagating modes. We use a set of units such that $L = 1$ and $\hbar v_\mathrm{F} = 1$. Further we take $E > 0$, which implies that $s = 1$ since the scattering, being elastic, cannot excite hole states which have $E < 0$. The equations to be solved numerically are given in appendix A.

The probability density current transported by the mode n is defined as

$$\boldsymbol{S}_n(x, y) = v_\mathrm{F}\psi_n^\dagger(x, y)\boldsymbol{\sigma}\psi_n(x, y). \tag{62}$$

Since the motion is transversely confined, what is needed is the probability density current along the x-direction, which reads

$$S_n(x) = v_\mathrm{F}\int_0^L \mathrm{d}y\, \psi_n^\dagger(x, y)\sigma_x\psi_n(x, y). \tag{63}$$

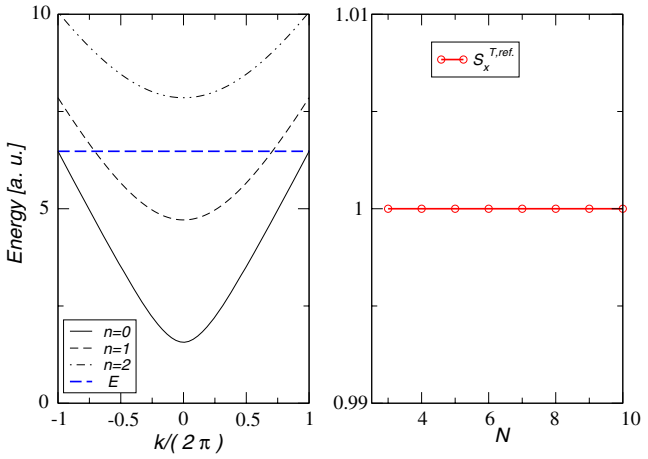

Figure 7. Left panel: energy levels for $n = 0, 1, 2$ and $k = 2\pi$. This leads to $N_p = 1$. Right panel: sum rule (64) for $N_p = 1$ as a function of $N = 3, 4, \ldots, 10$. We have depicted only odd values of N, such that the total number of odd and even terms is the same ($n = 0$ is considered even), but our results are independent of this choice.

Using definition (63), the total reflected flux density, $S_x^{\mathrm{T,refl}}$, obeys the sum rule

$$S_x^{\mathrm{T,refl}} = |r_{0,0}|^2 + \sum_{m=1}^{N_p} \frac{\cos\beta_m}{\cos\beta_0}|r_{0,m}|^2 = 1, \tag{64}$$

with

$$\beta_n = \arctan\frac{q_n}{k_n}, \tag{65}$$

with both q_n and k_n real. In agreement with our expectations, the sum rule is better fulfilled the larger N is, although modest values of N do a good job as well. In fact, in the right panel of figure 7 one can see that the sum rule is fulfilled even considering only one evanescent mode ($N = 3$).

In figure 8 we study, for the particular mode occupation defined in the left panel of figure 7, the evolution of the coefficients $r_{0,n}$ as a function of N. We write each coefficient $r_{0,p}$ as $r_{0,p} = |r_{0,p}|\,\mathrm{e}^{\mathrm{i}\alpha_{0,p}}$. In figure 8, we plot the square of the modulus of $r_{0,p}$ (left panels) and the corresponding phase $\alpha_{0,p}$ (right panels), separating the cases for which $p = 0, 1$ (propagating modes), which are represented in the two top panels, from those where $p \geqslant 2, \ldots, 7$ (evanescent modes), which we represent in the two bottom panels. A beautiful result emerges from this study. The wall introduces mode mixing and generates evanescent waves, whose contribution to the total wavefunction diminishes upon increasing p. This result is quite different from that for Schrödinger electrons, where no mode mixing takes place. The fundamental reason is due to the fact that for Schrödinger electrons the transverse wavefunction is the same for the incoming and outgoing waves. For Dirac electrons, on the contrary, the spinor of the incoming and outgoing waves changes due to its dependence on either the incoming or outgoing momentum.

Had we tried to force the solution of the problem using only one incoming and one outgoing propagating mode, with the same k value, we would have obtained the trivial solution $k = 0$. This statement is easily proved as follows: we make the

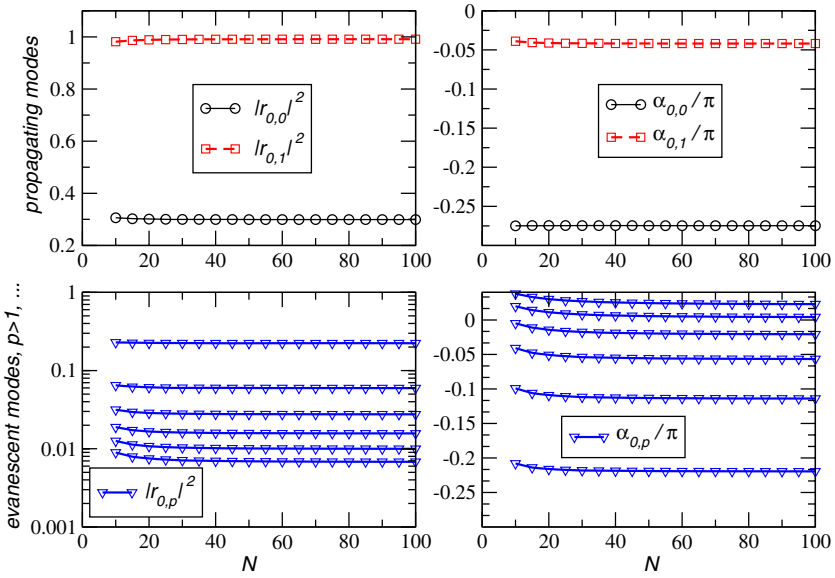

Figure 8. Top panels: evolution of $|r_{0,0}|^2$ and $|r_{0,1}|^2$ as a function of N (left); evolution of the phases $\alpha_{0,0}$ and $\alpha_{0,1}$ as a function of N (right). Bottom panels: the same as before but now for $|r_{0,p}|^2$ (left) and for $\alpha_{0,p}$ (right), considering $p = 2, \ldots, 7$.

assumption that the total wavefunction should be a sum of two terms of the form

$$\Psi_{n,k}(x, y) = \begin{pmatrix} \Psi_1(x, y) \\ \Psi_2(x, y) \end{pmatrix} = \left[\begin{pmatrix} 1 \\ z_{n,k} \end{pmatrix} e^{iq_n y} + \begin{pmatrix} z_{n,k} \\ 1 \end{pmatrix} e^{-iq_n y} \right] e^{ikx} + \left[\begin{pmatrix} 1 \\ z_{n,-k} \end{pmatrix} e^{iq_n y} + \begin{pmatrix} z_{n,-k} \\ 1 \end{pmatrix} e^{-iq_n y} \right] e^{-i(kx-2\delta)}, \quad (66)$$

where the phase shift δ was introduced. Let us now impose the boundary condition (52) on the wavefunction (66). Working out the calculation, one obtains two conditions that must be fulfilled simultaneously

$$\cos\delta \pm \sin(\beta_{n,k} - \delta) = 0, \quad (67)$$

with $\beta_{n,k}$ defined from $z_{n,k} = e^{i\beta_{n,k}}$. It is clear that the two conditions in equation (67) cannot be satisfied, in general, at the same time, which precludes the proposal of equation (66) as a solution to the problem. In fact, the two conditions given by equation (67) are equivalent to

$$\delta = \frac{\pi}{2} + \ell\pi \wedge \delta = \beta_{n,k} + \ell\pi, \qquad \ell = 0, 1, 2, \ldots, \quad (68)$$

which can only be true if $2\beta_{n,k} = \pi$, a situation that occurs only if

$$\arctan\frac{q_n}{k} = \frac{\pi}{2}, \quad (69)$$

which finally is true only in the trivial case $k = 0$. This means that the wavefunction has no x dependence and that the electronic density is $\rho(x, y) = \Psi^{\dagger}_{n,k}(x, y)\Psi_{n,k}(x, y) = 1/L$, constant everywhere (for finite m the density does show oscillations inside the box [89]). The exact solution of the square billiard with infinite mass confinement is therefore a quite elusive problem [91].

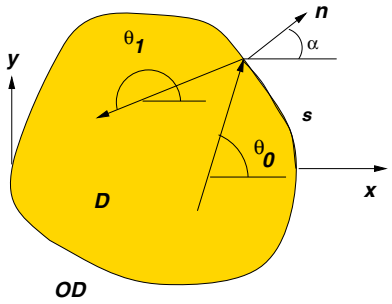

Figure 9. Domain D with the boundary parametrized by s. Figure adapted from [91]. The incident and reflected wave at s are both shown.

5. Confinement of Dirac fermions in quantum dots

Let us now consider the confinement of Dirac fermions in quantum dots. Naively one would expect that the rectangular dot would have a simple solution (as it has in the Schrödinger case), since the wavefunction of the confined Dirac electrons (by an infinite mass term) in a strip can be written in terms of elementary trigonometric functions. In fact this is not the case. The only known case so far of an integrable Dirac dot (billiard), subjected to infinite mass confinement, is the circular one. In order to solve this problem one needs the boundary condition obeyed by the wavefunction at the dot boundary. This was worked out by Berry and Mondragon [91] and the geometry they used is represented in figure 9. They considered a quantum dot represented by a domain D of arbitrary shape, separated by an outside region that we denote OD. The boundary of the domain D is parametrized by an length arc $s(\alpha)$, where the vector normal to the surface of the dot at s is given by

$$\boldsymbol{n}(s) = \cos\alpha(s)\vec{e}_x + \sin\alpha(s)\vec{e}_y. \quad (70)$$

Imposing the condition of zero flux perpendicular to the wall of the dot one obtains

$$\frac{\psi_2}{\psi_1} = \mathrm{i}B\,\mathrm{e}^{\mathrm{i}\alpha(s)}. \tag{71}$$

The constant B is determined by working out the study of a reflecting wave at the boundary of the dot, when the mass in the region OD obeys the condition $M \to \infty$. The final result is $B = 1$ [91], and the detailed calculation can be found in appendix B.

5.1. The circular dot with zero magnetic field

Let us first write the free solutions of the Dirac equation in polar coordinates r and φ. In this coordinates the Dirac Hamiltonian and the wavefunction read [95, 73, 96–98]

$$H = -\mathrm{i}\hbar v_\mathrm{F}\begin{pmatrix} 0 & \mathrm{e}^{-\mathrm{i}\varphi}\left(\partial_r - \frac{\mathrm{i}}{r}\partial_\varphi\right) \\ \mathrm{e}^{\mathrm{i}\varphi}\left(\partial_r + \frac{\mathrm{i}}{r}\partial_\varphi\right) & 0 \end{pmatrix}, \tag{72}$$

and

$$\Psi_{k,m}(r,\varphi) = \begin{pmatrix} J_m(rk)\,\mathrm{e}^{\mathrm{i}m\varphi} \\ s\mathrm{i}J_{m+1}(rk)\,\mathrm{e}^{\mathrm{i}(m+1)\varphi} \end{pmatrix}, \tag{73}$$

respectively, where $J_m(x)$ is the Bessel function of integer order m. A detailed derivation of these results is given in appendix C. In order to obtain the eigenvalues of the electrons in the dot one has to apply the boundary condition (71). Note that because one has a circular dot $\alpha(s) = \varphi$. This latter property makes it possible to satisfy the boundary condition (71) with the wavefunction (73) alone. In fact, for a dot of radius R, one has

$$s\mathrm{i}J_{m+1}(Rk)\,\mathrm{e}^{\mathrm{i}(m+1)\varphi} = J_m(Rk)\,\mathrm{e}^{\mathrm{i}m\varphi}\mathrm{i}\,\mathrm{e}^{\mathrm{i}\varphi} \Leftrightarrow sJ_{m+1}(Rk) = J_m(Rk), \tag{74}$$

whose numerical solution gives the value of kR for a given s and m, and from this the energy levels are computed using $E_{s,m,j} = s\hbar v_\mathrm{F}k_{s,m,j}$. The eigenvalues $E_{s,m,j}$ are defined by three quantum numbers, s, m and j, where j represents the ascending order of the values of kR that satisfy (74), for a given s and m. In section 5.2 we give numerical results for the energy eigenvalues.

5.2. The circular dot in a finite magnetic field

Let us now see how we can adapt our formalism to address the calculation of the energy eigenvalues of a circular dot in a magnetic field, that is we want to study the formation of Landau levels in reduced geometries (amusingly enough, the first calculation of Landau levels using the Dirac equation is as old as quantum mechanics itself [99], a result that was forgotten by graphene scientists). Experimentally this situation has been realized in [100]. The cyclotron motion of bulk graphene was discussed in [101].

The Hamiltonian (72) was written for a single Dirac cone. As shown in appendix C, the Hamiltonian for the two Dirac cones can be written using an additional quantum number $\kappa = \pm$, associated with the valley index, reading

$$H_\kappa = -\hbar v_\mathrm{F}\begin{pmatrix} 0 & \mathrm{i}\partial_x + \kappa\partial_y \\ \mathrm{i}\partial_x - \kappa\partial_y & 0 \end{pmatrix}. \tag{75}$$

In this section we do not use the infinite mass boundary condition, but introduce the zigzag type boundary condition. This will allow us to consider the presence edge states [102]. As we will show in section 5.3, these states are always present in graphene quantum dots. Recalling figure 1, one sees that at the zigzag edge only one type of carbon atom (either A or B) is present. The boundary condition at a zigzag edge with, say, only B atoms present, requires that the amplitude of the wavefunction at the A atoms to be zero; we therefore have the condition

$$\psi_1(R,\varphi) = 0. \tag{76}$$

In the following we will choose the boundary condition defined by equation (76), for which the wavevector is quantized as $k = z_{mj}/R$, where z_{mj} denotes the jth root of the mth Bessel function, $J_m(z_{mj}) = 0$.

A magnetic field $\vec{B} = B\vec{e}_z$, perpendicular to the graphene sheet, gives rise to a vector potential, which in polar coordinates reads $\vec{A} = A_\varphi\vec{e}_\varphi$, and, using the Gauss theorem, one obtains $2\pi rA_\varphi = \pi r^2 B$. Making the traditional minimal coupling of the charged electrons to the vector potential, the Hamiltonian has the form

$$H_\kappa = -\mathrm{i}\hbar v_\mathrm{F}\begin{pmatrix} 0 & \mathrm{e}^{-\mathrm{i}\kappa\varphi}\left(\partial_r - \kappa\frac{\mathrm{i}}{r}\partial_\varphi + \kappa\frac{\pi Br}{\Phi_0}\right) \\ \mathrm{e}^{\mathrm{i}\kappa\varphi}\left(\partial_r + \kappa\frac{\mathrm{i}}{r}\partial_\varphi - \kappa\frac{\pi Br}{\Phi_0}\right) & 0 \end{pmatrix}, \tag{77}$$

where $\Phi_0 = h/e \simeq 4136\ \mathrm{T\,nm^2}$ denotes the elementary flux quantum and $-e$ is the electron charge. We now make the observation that the trial function

$$\Psi_{m,\kappa}(r,\varphi) = \begin{pmatrix} \psi^1_{m,\kappa}(r)\,\mathrm{e}^{\mathrm{i}m\varphi} \\ \psi^2_{m,\kappa}(r)\,\mathrm{e}^{\mathrm{i}(m+\kappa)\varphi} \end{pmatrix}, \tag{78}$$

renders the eigenvalue problem a one-dimensional one, with the radial Hamiltonian given by

$$H_\kappa = -\mathrm{i}\hbar v_\mathrm{F}\begin{pmatrix} 0 & \partial_r + \frac{\kappa m+1}{r} + \kappa\frac{\pi Br}{\Phi_0} \\ \partial_r - \frac{\kappa m}{r} - \kappa\frac{\pi Br}{\Phi_0} & 0 \end{pmatrix}. \tag{79}$$

Let us make the substitution $\psi^i = \tilde{\psi}^i/\sqrt{r}$ $(i = 1, 2)$ in the eigenvalue equation defined by the Hamiltonian (79), with the radial spinor wavefunction having the form $\psi = (\psi^1, \psi^2)$. This substitution was considered before in the exact solution of the Coulomb problem in the 2 + 1-dimensional Dirac equation [103] and also in [96]. This procedure leads to a more symmetric eigenproblem of the form

$$-\mathrm{i}\hbar v_\mathrm{F}\left[\partial_r\tilde{\psi}^2_{m,\kappa}(r) + \left(\frac{\kappa m + 1/2}{r} + \kappa\frac{\pi Br}{\Phi_0}\right)\tilde{\psi}^2_{m,\kappa}(r)\right] = E\tilde{\psi}^1_{m,\kappa}(r), \tag{80}$$

$$-\mathrm{i}\hbar v_\mathrm{F}\left[\partial_r\tilde{\psi}^1_{m,\kappa}(r) - \left(\frac{\kappa m + 1/2}{r} + \kappa\frac{\pi Br}{\Phi_0}\right)\tilde{\psi}^1_{m,\kappa}(r)\right] = E\tilde{\psi}^2_{m,\kappa}(r). \tag{81}$$

We want to solve the eigenproblem defined by (80) and (81) by diagonalizing a Hermitian matrix. To this end let us look at the problem of a dimerized one-dimensional tight-binding model, such as that represented in figure 10. The relevance of

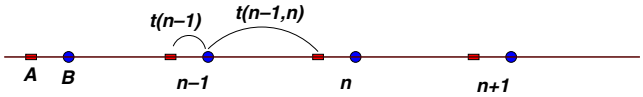

Figure 10. Representation of a dimerized chain of atoms A and B. Within the unit cell n the hopping is $t(n)$ and between the unit cells n and $n+1$ the hopping is $t(n, n+1)$. They can be functions of the unit cell position n.

this interlude will be apparent in a moment. The Hamiltonian for the depicted system is

$$H = \sum_n [t(n)|nA\rangle\langle nB| + t(n, n+1)|nB\rangle\langle n+1A| + \text{h.c.}], \tag{82}$$

and the wavefunction is written as

$$|\Psi\rangle = \sum_n (a_n|nA\rangle + b_n|nB\rangle). \tag{83}$$

The eigenvalue equation $H|\Psi\rangle = E|\Psi\rangle$ can be reduced to the solution of the linear homogeneous system

$$b_n t(n) + b_{n-1} t(n-1, n) = a_n E, \tag{84}$$

$$a_n t(n) + a_{n+1} t(n, n+1) = b_n E. \tag{85}$$

Introducing the simplifying notation $t(n, n+1) = t'(n)$, the above eigensystem reads

$$b_n t(n) + b_{n-1} t'(n-1) = a_n E, \tag{86}$$

$$a_n t(n) + a_{n+1} t'(n) = b_n E. \tag{87}$$

We note that equations (86) and (87) pose a well-defined numerical problem for well-behaved functions $t(n)$ and $t'(n)$. Let us now see what kind of continuous model follows from this lattice problem. Notice that, since the model under consideration has a valence and a conduction band, in the case where we have one electron per site the relevant energies are around zero. In this case, the amplitudes a_n and b_n oscillate between positive and negative values within a lattice unit cell. In order to construct a well-defined continuous model we need to subtract this oscillatory behaviour, making the replacement $a_n = \mathrm{i}(-)^n \tilde{a}_n$ and $b_n = (-)^n \tilde{b}_n$. This produces the set of equations

$$-\mathrm{i}[\tilde{b}_n t(n) - \tilde{b}_{n-1} t'(n-1)] = \tilde{a}_n E, \tag{88}$$

$$-\mathrm{i}[-\tilde{a}_n t(n) + \tilde{a}_{n+1} t'(n)] = \tilde{b}_n E. \tag{89}$$

Defining now $T(n) = [t(n) + t'(n)]/2$ and $\Delta(n) = [t(n) - t'(n)]/2$ and recalling that the first order derivatives can be approximated by

$$\partial_r \tilde{a} \to [\tilde{a}(r_{n+1}) - \tilde{a}(r_n)]/\Delta r, \tag{90}$$

$$\partial_r \tilde{b} \to [\tilde{b}(r_n) - \tilde{b}(r_{n-1})]/\Delta r. \tag{91}$$

and that $\Delta r = R/N_l$, $r_n = Rn/N_l$ a discretized position vector, with R the length of the chain (which will correspond later to the radius of the dot), $n = 1, \ldots, N_l$, and N_l the number of points in which the length R was discretized, we obtain

$$-\mathrm{i}[T(r)\Delta r \partial_r \tilde{b} + 2\Delta(r)\tilde{b}] = \tilde{a}E, \tag{92}$$

$$-\mathrm{i}[T(r)\Delta r \partial_r \tilde{a} - 2\Delta(r)\tilde{a}] = \tilde{b}E. \tag{93}$$

We can thus make the following addition to the continuous model:

$$T(r) = \frac{\hbar v_\mathrm{F}}{\Delta r}, \tag{94}$$

$$\pm 2\Delta(r) = \frac{\kappa m + 1/2}{r} + \kappa \frac{\pi B r}{\Phi_0} = Q(r). \tag{95}$$

The ambiguity introduced by the $\pm$ sign in equation (95) can be settled by looking at the bulk limit of the problem. The choice that gives the correct answer is $t'(n) = T(r) + Q(r)/2$ and $t(n) = T(r) - Q(r)/2$. If we assume that the wall of the dot is located at $n = N_l$, then the boundary condition (76) is imposed considering $\tilde{\psi}^1_{N_l} = 0$. In order to keep the problem particle–hole symmetric, we consider the case where the effective chain problem has N_l unit cells.

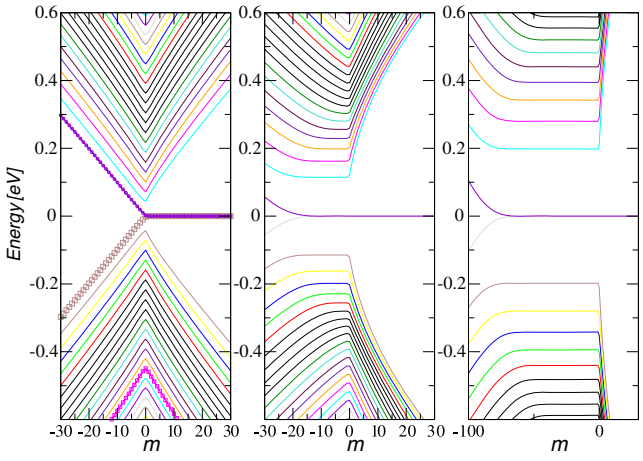

Figure 11. Forty energy levels of a circular graphene quantum dot in a finite magnetic field as a function of the angular momentum quantum number m. The radius of the dot is $R = 70$ nm, three magnetic fields were used, $B = 1$, 10, 30 T (from left to right), and $\kappa = 1$. The two surface states (for $m > 0$) are represented using squares and circles.

In figure 11 we represent the numerical solution of equations (86) and (87). It is clear that at small fields the bands are essentially symmetric for positive and negative m values, a property that comes from the fact that exchanging m by $-m$ in the Dirac equation only replaces the role of ψ^1_n and ψ^2_n. With a finite magnetic field the situation changes. Also seen is the presence of a dispersive edge state. The dispersive part, occurring for positive m, is dependent on the Dirac point. Note the appearance of the zero energy Landau level upon increasing the magnetic field. The different behaviour, for large fields, shown by the energy levels for positive and negative m is associated with the amount of angular momentum induced by the magnetic field.

Let us now discuss how to include the Coulomb interaction in the calculation. This is important because the screening in the dot may not be very effective and because

the dot may be working under a regime where it has a net charge density (charged dot). The situation of a charged dot is represented in figure 12. The gate potential V_g induces either holes or electrons in the dot. This causes a situation where the dot is charged, since the neutrality case occurs when the chemical potential is at the Dirac point. If we take the graphene to be at a potential V_g then the charges accumulated in the metal–insulator interface have to be at zero potential. This means that one must use a set of images charges at a distance t from the interface with exactly the same spatial density of that formed in the graphene dot. We then have to describe the Coulomb interaction of an electron in the dot with both the self-consistent charge density in the graphene and its image underneath the metal–insulator interface [107]. The simplest way to include the effect of Coulomb repulsion is by using the self-consistent Hartree approximation. We analyse here the effects induced by increasing the number of electrons in the dot using the Hartree approximation [104]. The self-consistent Hartree potential describes, within a mean field approximation, the screening of charges within the dot. We assume that a half-filled dot is neutral, as the ionic charge compensates the electronic charge in the filled valence band. Away from half filling, the dot is charged. Then, an electrostatic potential is induced in its interior, and there is an inhomogeneous distribution of charge. We describe charged dots by fixing the chemical potential, and obtaining a self-consistent solution where all electronic states with lower energies than the Fermi energy are filled. From this calculation we obtain the Hartree electronic energy bands. The Hartree approximation should give a reasonable description when Coulomb blockade effects can be described as a rigid shift of the electrostatic potential within the dot [105, 106]. Using the same discretization procedure as before, the numerical equations to be solved now have the form

$$v_{\mathrm{H}}(n)a_n + b_n t(n) + b_{n-1}t'(n-1) = a_n E_{j,m}, \tag{96}$$

$$v_{\mathrm{H}}(n)b_n + a_n t(n) + a_{n+1}t'(n) = b_n E_{j,m}. \tag{97}$$

where the Hartree potential in the continuum, $v_{\mathrm{H}}(r)$, is given by

$$v_{\mathrm{H}}(r) = v_0 \int r'\,\mathrm{d}r'\,\mathrm{d}\varphi\,\mathcal{K}(\boldsymbol{r},\boldsymbol{r}',t) \simeq v_0 \frac{R}{N_l}\sum_{n'\neq n}\int_0^{2\pi} \mathrm{d}\varphi\, r'_n\,\mathcal{K}(\boldsymbol{r}_n,\boldsymbol{r}'_n,t), \tag{98}$$

and

$$\mathcal{K}(\boldsymbol{r},\boldsymbol{r}',t) = \frac{\rho(r')}{\sqrt{r^2+(r')^2-2rr'\cos\varphi}} - \frac{\rho(r')}{\sqrt{r^2+(r')^2-2rr'\cos\varphi+4t^2}} \tag{99}$$

with the parameter v_0 given by $v_0 = (e^2/4\pi\epsilon_0\epsilon)$ and $\rho(r_n)$ the electronic density at point r_n, computed from

$$\rho(r_n) = gC\sum_m \sum_{j_m\neq j_{m,\mathrm{spur.}}} [a^2_{n,m,j_m} + b^2_{n,m,j_m}]/r_n, \tag{100}$$

such that the sums over m and j_m are constrained to those energy levels such that $E_{m,j} \leqslant E_{\mathrm{F}}$ (note that the explicit dependence of a_n and b_n on m and j_m has been introduced in equation (100)), where E_{F} is the Fermi energy measured relative to the Dirac point, g is the spin and valley degeneracy and the constant C is given by the normalization condition on the disc, $C = (2\pi\,\Delta r)^{-1}$. The constraint in the j summation in equation (100) is due to the fact that the boundary conditions introduced by the finite tight-binding chain fails to reproduce accurately the boundary condition $\tilde{\psi}_i(r \to 0) \to 0$, introducing a spurious mode characterized by the quantum number $j_{m,\mathrm{spur.}} = N_l + 1$ for $m \geqslant 0$; in order for sensible results to be obtained these modes have to be removed.

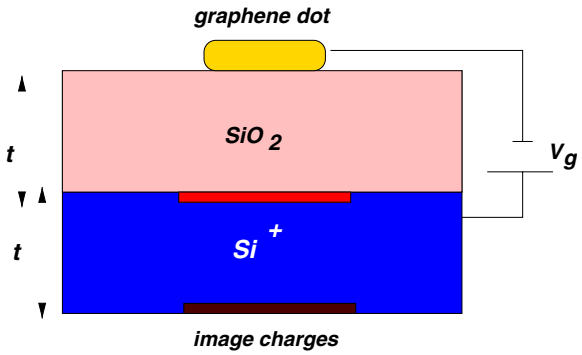

Figure 12. Lateral view of graphene FET. When the dot is gated the charge accumulates at the metal–insulator (Si^+–SiO_2) interface. The thickness of the insulator is t and the applied gate potential is V_g.

We note that the integral (98) is well behaved since the self-interaction has been excluded ($n \neq n'$). Further the $\rho(r_{n'})$ is independent of φ. The angular integral in equation (98) can be formally computed leading to

$$v_{\mathrm{H}}(n) = 4v_0\frac{R}{N_l}\sum_{n'\neq n}\left[\frac{r_{n'}\rho(r_{n'})}{r_n+r_{n'}}\mathbf{K}\left(\frac{4r_n r_{n'}}{(r_n+r_{n'})^2}\right) - \frac{r_{n'}\rho(r_{n'})}{\sqrt{(r_n+r_{n'})^2+4t^2}}\mathbf{K}\left(\frac{4r_n r_{n'}}{(r_n+r_{n'})^2+4t^2}\right)\right]. \tag{101}$$

with $\mathbf{K}(m)$ defined as

$$\mathbf{K}(m) = \int_0^1 \mathrm{d}x[(1-x^2)(1-mx^2)]^{-1/2}. \tag{102}$$

The elliptic integral $\mathbf{K}(m)$ can be approximated by an analytical function [108], which reduces the numerical effort. It is now clear that, due to the Hartree potential, the problem defined by equations (96) and (97) has to be solved self-consistently.

One should comment on the fact that for a large dot $R \gg t$ the contribution from $v_{\mathrm{H}}(\boldsymbol{r})$ essentially vanishes and the change of the bands due to the Hartree term is vanishingly small. On the contrary, for small dots $R \sim t$ and the Hartree renormalization of the electronic energy levels can be very important in the case of heavily charged dots.

In figure 13 we represent the energy bands of a quantum dot of radius $R = 100$ nm on top of a silicon oxide slab of thickness $t = 100$ nm. We used a gate voltage of $V_g = 2$ V, which corresponds to a Fermi energy of $E_{\mathrm{F}} = 0.077$ eV for the bulk system; the values of the magnetic field used were $B = 1$ T (top panels) and $B = 3.5$ T (bottom panels). It is

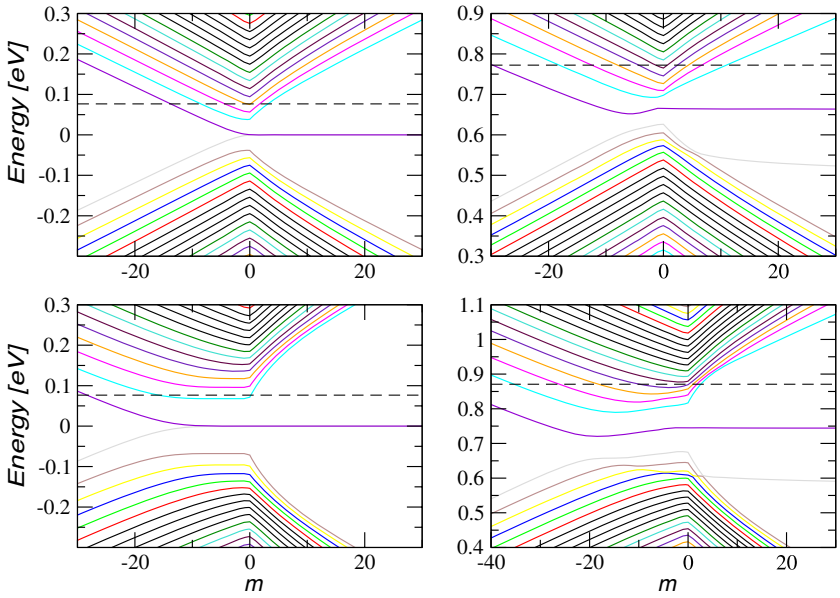

Figure 13. Independent and Hartree energy levels for a spherical quantum dot with $R = 100$ nm, on top of a silicon oxide slab of $t = 100$ nm ($\epsilon = 3.9$), for a Fermi energy $E_F = 0.077$ eV (represented by a dashed line). For $B = 1$ T, the number of electrons in the dot is $N_e = 166$ and the magnetic length is $\ell_B = 26$ nm; for $B = 3.5$ T, the number of electrons in the dot is $N_e = 178$ and the magnetic length is $\ell_B = 14$ nm. The left panels are the independent energy bands; the right ones are the Hartree bands. The top row is for $B = 1$ T. The lattice has $N_l = 100$.

clear that the Hartree bands are renormalized by the Coulomb interaction. In figure 14 we represent the self-consistent density, $\rho(r)$, and Hartree potential, $v_H(n)$, for two different values of the magnetic field. The parameters are those given in the caption of figure 13. The increase in the Hartree potential upon increasing B is due to the increase in the number of electrons in the dot.

We should comment that in our calculation we have not tried to keep the number of electrons fixed. This can easily be done, but increases the computational effort since the chemical potential has to be self-consistently determined. Instead, we have chosen to keep the Fermi energy constant, which, of course, leads to a change in the number of electrons in the dot with the variation of the magnetic field. Also the population of the surface states was not included in the calculation, using a criterion of computational simplicity. In a future study we shall relax these two constraints.

Another important aspect in quantum dot physics is that of confinement introduced by the potential creating the dot. The confinement potential can either be due to etching or to applied gates. In the case of dots or narrow channels described by the Schrödinger equation, a very popular confinement is that introduced by a parabolic potential [109], since it allows a simple analytical solution. We choose a confinement potential given by

$$V_{\rm conf}(r) = U_c(r/R)^4, \tag{103}$$

which rises smoothly from the centre of the dot. The prefactor U_c is the strength of the potential at the edge of the dot. As in the case of the Hartree potential, $V_{\rm conf}(r)$ enters in the diagonal part of the radial Hamiltonian. In figure 15 we give a comparison of the energy bands for $B = 10$ T. Comparing the left and the right panels of figure 15 we see that the Landau levels become dispersive with m due to the

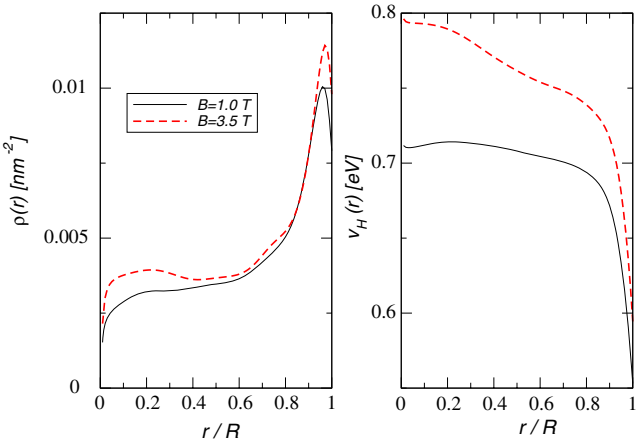

Figure 14. Self-consistent electronic density (left) and Hartree potential $v_H(n)$ (right) for the same parameters given in the caption of figure 13.

confinement, a result also found for Landau levels derived from the Schrödinger equation [109]. Interestingly, we see that the confinement also breaks the particle–hole symmetry of the problem, a result found previously for the ribbon problem [110].

5.3. The hexagonal and circular dots at the tight-binding level

In this section we want to address the question of whether graphene quantum dots will or will not have edge states, starting from the full solution of the tight-binding Hamiltonian (10). Edge states in graphene nanostructures are of particular importance since they can give rise to magnetism (see, for example, [111]). In order to access the low energy

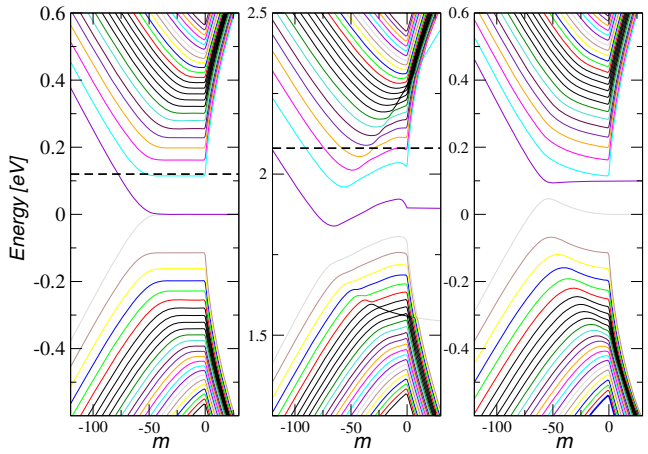

Figure 15. Energy spectrum of a graphene quantum dot at $B = 10$ T. From left to right: independent particle bands, Hartree bands and independent particle bands with the confinement potential (103). The parameters are $U_c = 0.1$ eV, $V_g = 5$ V, $E_F = 0.12$ eV; the remaining parameters are those used in figure 13. The magnetic length is $\ell_B = 8$ nm and the number of electrons in the dot is $N_e = 463$.

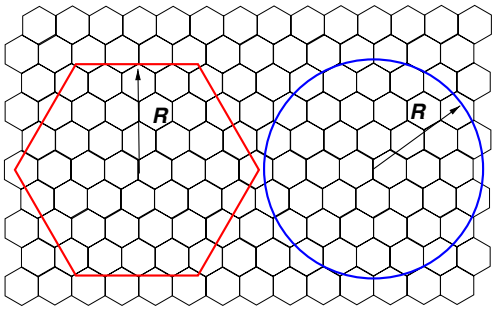

Figure 16. Representation of a graphene crystallite on top of which hexagonal or circular dots can be patterned. The size of the dot is defined by the length R.

density of states of dots with physically relevant sizes (bigger than 10 nm) a Lanczos technique is used, since the exact diagonalization of systems of this size becomes intractable. For a brief introduction to the Lanczos technique see, for example, [112].

We have chosen to diagonalize dots of *circular* and *hexagonal* shape with zigzag termination, such as those depicted in figure 16. Our numerical findings are represented in figure 17. It is clear that as the size of the dot grows larger the number of zero energy states increases, indicating the presence of zero energy edge states, even in circular geometry. It is also clear that the number of edge states is larger in the case of a hexagonal dot due to its perfect zigzag termination, such that each side of the hexagon has either a surplus of A or B atoms. When a finite t' is added to the Hamiltonian, the edge states become dispersive [40] and there is a reduction in the density of zero energy states (seen in the hexagonal dot).

6. Final comments

In this work a description of the confinement of Dirac electrons in nano-wires and quantum dots was given. It was shown that, in principle, it is possible to localize electronic modes in a spatial region of a nano-wire, using a p–n–p gate potential setup. The energy spectrum of quantum dots in a magnetic field was described taking into account both the effect of electron–electron interactions, at the Hartree level, and the effect of confining potentials. Exchange [113–115] can in principle be included in this study. The interesting aspects about this possibility are two-fold: first, the exchange energy for Dirac electrons is different from that for the two-dimensional electron gas described by the Schrödinger equation; second, and contrary to the Hartree potential, the exchange energy of the full electronic system has to be considered, since there is not an equivalent cancellation effect to that found in the Hartree potential between the ion background and the direct Coulomb energy of the valence electrons. These aspects will be pursued in a follow-up study [116].

Acknowledgments

NMRP, TS, and JMBLS acknowledge financial support from POCI 2010 via project PTDC/FIS/64404/2006 and from ESF via INSTANS. The authors thank Daniel Arovas, Antônio Castro Neto, Eduardo Castro, Francisco Guinea and Vitor Pereira for discussions; Andre Geim is acknowledged for suggestions.

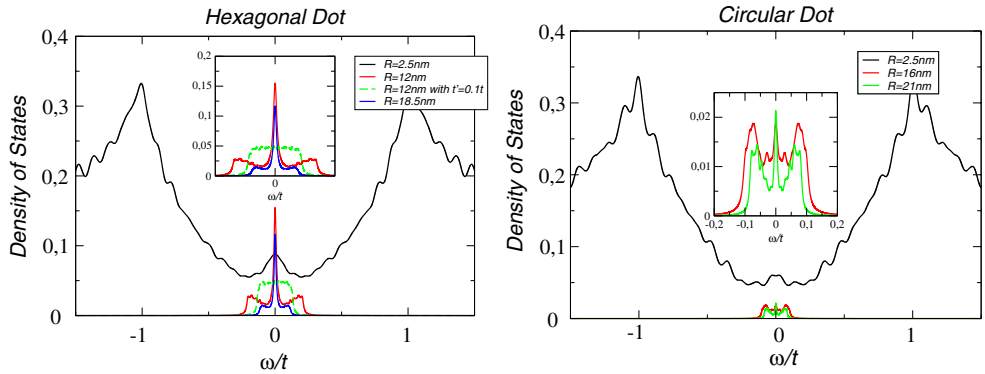

Figure 17. Density of states at low energies for hexagonal (left) and circular dots (right). The insets are a zoom in of the density of states close to the Dirac point. Dots of several sizes are represented.

Appendix A. Equations for the numerical solution of the scattering problem

Below we give the equations that were solved numerically when we studied the scattering problem by a wall of infinite mass. These are:

- $p = 0$:

$$\left[(1+\mathrm{i}z_0)+r_0(1+\mathrm{i}\tilde{z}_0)\right]+\frac{2}{\mathrm{i}\pi}\left[(z_0+\mathrm{i})+r_0(\tilde{z}_0+\mathrm{i})\right] + \sum_{m_{\mathrm{odd}}>0}\frac{-2}{\mathrm{i}m\pi}\left[r_m(1+\mathrm{i}\tilde{z}_m)\right] + \sum_{m_{\mathrm{even}}>0}\frac{2}{\mathrm{i}(m+1)\pi}\left[r_m(\tilde{z}_m+\mathrm{i})\right]=0, \tag{A.1}$$

- $p \neq 0$ and even:

$$r_p(1+\mathrm{i}\tilde{z}_p)+\frac{2}{\mathrm{i}(p+1)\pi}\left[(z_0+\mathrm{i})+r_0(\tilde{z}_0+\mathrm{i})\right] + \sum_{m_{\mathrm{odd}}>0}\frac{2}{\mathrm{i}(p-m)\pi}\left[r_m(1+\mathrm{i}\tilde{z}_m)\right] + \sum_{m_{\mathrm{even}}>0}\frac{2}{\mathrm{i}(p+m+1)\pi}\left[r_m(\tilde{z}_m+\mathrm{i})\right]=0, \tag{A.2}$$

  with the possibility of having $m = p$ in the m_{even} summation

- p odd

$$r_p(\tilde{z}_p+\mathrm{i})+-\frac{2}{\mathrm{i}p\pi}\left[(z_0+\mathrm{i})+r_0(\tilde{z}_0+\mathrm{i})\right] + \sum_{m_{\mathrm{odd}}>0}\frac{-2}{\mathrm{i}(p+1+m)\pi}\left[r_m(1+\mathrm{i}\tilde{z}_m)\right] + \sum_{m_{\mathrm{even}}>0}\frac{2}{\mathrm{i}(-p+m)\pi}\left[r_m(\tilde{z}_m+\mathrm{i})\right]=0, \tag{A.3}$$

with the possibility of having $m = p$ in the m_{odd} summation. It is clear that we can truncate this set of equations to obtain a set of N equations for the coefficients $r_0, \ldots, r_{N-1}$.

Appendix B. General boundary conditions in a quantum dot with infinite mass confinement

In this appendix we give all the details of how to obtain the boundary condition of the wavefunction at the wall of a quantum dot, with the confinement determined by the infinite mass condition. We must compute the wavefunction in the domain D due to a reflection at the boundary. We write the plane wave inside D as

$$\Psi_D = \begin{pmatrix}1\\ \mathrm{e}^{\mathrm{i}\theta_0}\end{pmatrix}\mathrm{e}^{\mathrm{i}\vec{k}_i\cdot\vec{r}} + R\begin{pmatrix}1\\ \mathrm{e}^{\mathrm{i}\theta_1}\end{pmatrix}\mathrm{e}^{\mathrm{i}\vec{k}_f\cdot\vec{r}}, \tag{B.1}$$

where from figure 9 we can conclude that $\theta_1 = \pi + 2\alpha - \theta_0$, and $\vec{k}_i$ and $\vec{k}_f$ are the momenta of the incident and reflected waves at the boundary of the dot. In order to calculate ψ_2/ψ_1 (which will make it possible to compute the value of B), we need to discover the value of the reflection coefficient R. We can accomplish this using the fact, required by the Dirac equation, that the components of the spinors must be continuous at the boundary.

First we solve the Dirac equation with a mass $Mv_{\mathrm{F}}^2 > E$. For the sake of simplicity, we use the normal and tangential coordinates n and s given by

$$n = x\cos\alpha + y\sin\alpha \qquad s = -x\sin\alpha + y\cos\alpha$$

which implies that,

$$\partial_x = (\partial_x n)\,\partial_n + (\partial_x s)\,\partial_s \qquad \partial_y = (\partial_y n)\,\partial_n + (\partial_y s)\,\partial_s$$

$$\partial_x = \cos\alpha\partial_n - \sin\alpha\partial_s \qquad \partial_y = \sin\alpha\partial_n + \cos\alpha\partial_s$$

resulting in

$$\partial_x \pm \mathrm{i}\partial_y = (\partial_n \pm \mathrm{i}\partial_s)\,\mathrm{e}^{\pm\mathrm{i}\alpha}.$$

Then, for a plane wave in the domain OD (complementary to D), $\Psi_{OD} = T\binom{u}{v}\mathrm{e}^{\mathrm{i}(k_n n + k_s s)}$ (where T stands for the transmission coefficient). Solving the Dirac equation explicitly we obtain

$$\Psi_{OD} = T\begin{pmatrix}1\\ \frac{E-Mv_{\mathrm{F}}^2}{\mathrm{i}\hbar v_{\mathrm{F}}(q-k)}\,\mathrm{e}^{\mathrm{i}\alpha}\end{pmatrix}\mathrm{e}^{\mathrm{i}ks-qn}, \tag{B.2}$$

where we have defined

$$k_n = \mathrm{i}q = \mathrm{i}\sqrt{\frac{M^2v_{\mathrm{F}}^4 - E^2}{\hbar^2 v_{\mathrm{F}}^2} + k^2}$$

and chosen the solution that decays for $r \to +\infty$. Further we identified $k_n = \mathrm{i}q$ and $k_s = k$. Imposing the continuity of the wavefunctions (B.1) and (B.2) at the boundary of the dot, one obtains

$$1 + R = T, \qquad \mathrm{e}^{\mathrm{i}\theta_0} + R\,\mathrm{e}^{\mathrm{i}\theta_1} = T\mathrm{i}\,\mathrm{e}^{\mathrm{i}\alpha}.$$

Replacing the value of R in equation (B.1), the wavefunction in the dot reads

$$\Psi_D = \frac{1}{\sqrt{2}}\begin{pmatrix}1\\ \mathrm{e}^{\mathrm{i}\theta_0}\end{pmatrix}\mathrm{e}^{\mathrm{i}\vec{k}_i\cdot\vec{r}} - \frac{1+\mathrm{i}\,\mathrm{e}^{-\mathrm{i}(\alpha-\theta_0)}}{1-\mathrm{i}\,\mathrm{e}^{\mathrm{i}(\alpha-\theta_0)}}\frac{1}{\sqrt{2}}\begin{pmatrix}1\\ \mathrm{e}^{\mathrm{i}\theta_1}\end{pmatrix}\mathrm{e}^{\mathrm{i}\vec{k}_f\cdot\vec{r}},$$

which, after some simple manipulations, allows us to conclude that

$$\frac{\psi_2}{\psi_1} = \mathrm{i}\,\mathrm{e}^{\mathrm{i}\alpha}$$

and therefore $B = 1$.

Appendix C. The Dirac equation in polar coordinates

To treat problems with circular symmetry, the partial derivatives with respect to Cartesian coordinates shall be written in polar coordinates (r, φ). For the x-coordinate, the product rule yields $\partial_x = (\mathrm{d}r/\mathrm{d}x)_y\partial_r + (\partial\varphi/\partial x)_y\partial_\varphi$, where the derivatives are taken for fixed y. The first derivative is obtained using $r = \sqrt{x^2+y^2}$. The second one uses $\tan\varphi = y/x$ and thus $(1/\cos^2\varphi)\partial_\varphi = -(y/x^2)\partial_x$. This gives

$$\partial_x = \cos\varphi\partial_r - \frac{\sin\varphi}{r}\partial_\varphi, \tag{C.1}$$

and analogously

$$\partial_y = \sin\varphi\partial_r + \frac{\cos\varphi}{r}\partial_\varphi. \tag{C.2}$$

The Hamiltonian thus reads

$$H_\kappa = -\mathrm{i}\hbar v_\mathrm{F}\begin{pmatrix} 0 & \mathrm{e}^{-\mathrm{i}\kappa\varphi}(\partial_r - \kappa\frac{\mathrm{i}}{r}\partial_\varphi) \\ \mathrm{e}^{\mathrm{i}\kappa\varphi}(\partial_r + \kappa\frac{\mathrm{i}}{r}\partial_\varphi) & 0 \end{pmatrix}, \tag{C.3}$$

where we have introduced the additional quantum number κ, to account for the two non-equivalent Dirac points. Let us now define the operators

$$L_+ \equiv \mathrm{e}^{\mathrm{i}\varphi}\left(\partial_r + \frac{\mathrm{i}}{r}\partial_\varphi\right), \tag{C.4}$$

$$L_- \equiv -\mathrm{e}^{-\mathrm{i}\varphi}\left(\partial_r - \frac{\mathrm{i}}{r}\partial_\varphi\right), \tag{C.5}$$

which acting on the product of a Bessel function of integer order m, $J_m(kr)$, and a complex exponential, $\mathrm{e}^{\mathrm{i}m\varphi}$, produce $L_\pm J_m(kr)\,\mathrm{e}^{\mathrm{i}m\varphi} = -kJ_{m\pm1}(kr)\,\mathrm{e}^{\mathrm{i}(m\pm1)\varphi}$. This last result leads to the construction of the wavefunction of the free problem in the form given in equation (73). In addition, the following commutators $[L_\varphi, L_\pm] = \pm L_\pm$ and $[L_+, L_-] = 0$ allow us to interpret the operators $L_\pm$ as rising and lowering operators of the angular momentum.

Finally we note that if we consider a ring instead of a disc it is possible to add a flux through the ring, introducing a vector potential $\vec{A}_\Phi = (\Phi/2\pi r)\vec{e}_\varphi$. The full Hamiltonian with both a perpendicular magnetic field and the magnetic flux through the ring is given by

$$H_\kappa = -\mathrm{i}\hbar v_\mathrm{F}\begin{pmatrix} 0 & \mathrm{e}^{\mathrm{i}\kappa\varphi}\left(\partial_r + \kappa\frac{1}{r}\left(\mathrm{i}\partial_\varphi - \frac{\Phi}{\Phi_0}\right) - \kappa\frac{\pi Br}{\Phi_0}\right) \\ \mathrm{e}^{-\mathrm{i}\kappa\varphi}\left(\partial_r - \kappa\frac{1}{r}\left(\mathrm{i}\partial_\varphi - \frac{\Phi}{\Phi_0}\right) + \kappa\frac{\pi Br}{\Phi_0}\right) & 0 \end{pmatrix}, \tag{C.6}$$

and its numerical solution can be accommodated within the explained method.

References

[1] Novoselov K S, Geim A K, Morozov S V, Jiang D, Zhang Y, Dubonos S V, Grigorieva I V and Firsov A A 2004 *Science* **306** 666

[2] Novoselov K S, Jiang D, Booth T, Khotkevich V V, Morozov S M and Geim A K 2005 *Proc. Natl Acad. Sci.* **102** 10451

[3] Oshima C and Nagashima A 1997 *J. Phys.: Condens. Matter* **9** 1

[4] Castro Neto A H, Guinea F and Peres N M R 2006 *Phys. World* **11** 33

[5] Geim A K and Novoselov K S 2007 *Nat. Mater.* **6** 183

[6] Katsnelson M I 2007 *Mater. Today* **10** 20

[7] Geim A K and MacDonald A H 2007 *Phys. Today* **60** 35

[8] Geim A K and Kim P 2008 *Sci. Am.* (April) 90

[9] Castro Neto A H, Guinea F, Peres N M R, Novoselov K S and Geim A K 2009 *Rev. Mod. Phys.* **81** 109
Castro Neto A H, Guinea F, Peres N M R, Novoselov K S and Geim A K 2007 arXiv:0709.1163v2

[10] Beenakker C W 2008 *Rev. Mod. Phys.* **80** 1337
Beenakker C W 2007 arXiv:0710.3848v2

[11] Booth T J, Blake P, Nair R R, Jiang Da, Hill E W, Bangert U, Bleloch A, Gass M, Novoselov K S, Katsnelson M I and Geim A K 2008 *Nano Lett.* **8** 2442

[12] Hernandez Y, Nicolosi V, Lotya1 M, Blighe1 F M, Sun Z, De1 S, McGovern I T, Holland B, Byrne M, Gun'Ko Y K, Boland J J, Niraj P, Duesberg G, Krishnamurthy S, Goodhue R, Hutchison J, Scardaci V, Ferrari A C and Coleman J N 2008 *Nat. Nanotechnol.* **3** 563

[13] Li X, Zhang G, Bai X, Sun X, Wang X, Wang E and Dai H 2008 *Nat. Nanotechnol.* **3** 538

[14] Yoshimura S and Chang R P H (ed) 1998 *Supercarbon: Synthesis, Properties and Applications* (Berlin: Springer)

[15] Chung D D L 2002 *J. Mater. Sci.* **37** 1

[16] Field J E (ed) 1992 *Properties of Natural and Synthetic Diamond* (San Diego, CA: Academic)

[17] Barth A and Marx W 2008 arXiv:0808.3320

[18] Lee C, Wei X, Kysar J W and Honel J 2008 *Science* **321** 385

[19] Balandin A A, Ghosh S, Bao W, Calizo I, Teweldebrhan D, Miao F and Lau C N 2008 *Nano Lett.* **8** 902

[20] Bunch J S, Verbridge S S, Alden J S, van der Zande A M, Parpia J M, Craighead H G and McEuen P L 2008 arXiv:0805.3309v1

[21] Morozov S V, Novoselov K S, Katsnelson M I, Schedin F, Elias D C, Jaszczak J A and Geim A K 2008 *Phys. Rev. Lett.* **100** 016602

[22] Bolotin K I, Sikes K J, Jiang Z, Klima M, Fudenberg G, Hone J, Kim P and Stormer H L 2008 *Solid State Commun.* **146** 351

[23] Peres N M R, Guinea F and Castro Neto A H 2006 *Phys. Rev.* B **73** 195411
Peres N M R, Guinea F and Castro Neto A H 2006 *Phys. Rev.* B **73** 239902

[24] Lin Y-M, Perebeinos V, Chen Z and Avouris P 2008 *Phys. Rev.* B **78** 161409(R)

[25] Sidorov A, Mudd D, Sumanasekera G, Ouseph P J, Jayanthi C S and Wu S-Y 2008 arXiv:0808.1577v1

[26] Ohta T, Bostwick A, Seyller T, Horn K and Rotenberg E 2006 *Science* **313** 951

[27] Mucha-Kruczyński M, Tsyplyatyev O, Grishin A, McCann E, Fal'ko V I, Bostwick A and Rotenberg E 2008 *Phys. Rev.* B **77** 195403

[28] Zhou S Y, Gweon G-H, Fedorov A V, First P N, de Heer W A, Lee D-H, Guinea F, Castro Neto A H and Lanzara A 2007 *Nat. Mater.* **6** 770

[29] Zhou S Y, Siegel D A, Fedorov A V, El Gabaly F, Schmid A K, Castro Neto A H, Lee D-H and Lanzara A 2008 *Nat. Mater.* **7** 259

[30] Deacon R S, Chuang K-C, Nicholas R J, Novoselov K S and Geim A K 2007 *Phys. Rev.* B **76** 081406

[31] Peres N M R, Lopes dos Santos J M B and Stauber T 2007 *Phys. Rev.* B **76** 073412

[32] Stauber T, Peres N M R and Guinea F 2007 *Phys. Rev.* B **76** 205423

[33] Lofwander T and Fogelstrom M 2007 *Phys. Rev.* B **76** 193401

[34] Trushin M and Schliemann J 2007 *Phys. Rev. Lett.* **99** 216602

[35] Du X, Skachko I, Barker A and Andrei E Y 2008 *Nat. Nanotechnol.* **3** 491

[36] Adam S and Das Sarma S 2008 *Solid State Commun.* **146** 356

[37] Stauber T, Peres N M R and Castro Neto A H 2008 *Phys. Rev.* B **78** 085418

[38] McChesney J L, Bostwick A, Ohta T, Emtsev K, Seyller T, Horn K and Rotenberg E 2008 arXiv:0809.4046

[39] Peres N M R and Stauber T 2008 *Int. J. Mod. Phys.* B **22** 2529

[40] Peres N M R, Guinea F and Castro Neto A H 2006 *Phys. Rev.* B **73** 125411

[41] Tworzydlo J, Trauzettel B, Titov M, Rycerz A and Beenakker C W J 2006 *Phys. Rev. Lett.* **96** 246802

[42] Katsnelson M I 2006 *Eur. Phys. J.* B **51** 157

[43] Ziegler K 2007 *Phys. Rev.* B **75** 233407

[44] Miao F, Wijeratne S, Zhang Y, Coskun U C, Bao W and Lau C N 2007 *Science* **317** 1530
[45] Danneau R, Wu F, Craciun M F, Russo S, Tomi M Y, Salmilehto J, Morpurgo A F and Hakonen P J 2008 *Phys. Rev. Lett.* **100** 196802
[46] Hill W E, Geim A K, Novoselov K, Schedin F and Blake P 2006 *IEEE Trans. Magn.* **42** 2694
[47] Cho S, Chen Y-F and Fuhrer M S 2007 *Appl. Phys. Lett.* **91** 123105
[48] Tombros N, Jozsa C, Popinciuc M, Jonkman H T and van Wees B J 2007 *Nature* **448** 571
[49] Jozsa C, Popinciuc M, Tombros N, Jonkman H T and van Wees B J 2008 arXiv:0802.2628v2
[50] Li Z Q, Henriksen E A, Jiang Z, Hao Z, Martin M C, Kim P, Stormer H L and Basov D N 2008 *Nat. Phys.* **4** 532
[51] Li Z Q, Henriksen E A, Jiang Z, Hao Z, Martin M C, Kim P, Stormer H L and Basov D N 2008 arXiv:0807.3776v1
[52] Gusynin V P, Sharapov S G and Carbotte J P 2007 *Int. J. Mod. Phys.* B **21** 4611
[53] Nair R R, Blake P, Grigorenko A N, Novoselov K S, Booth T J, Stauber T, Peres N M R and Geim A K 2008 *Science* **320** 1308
[54] Stauber T, Peres N M R and Geim A K 2008 *Phys. Rev.* B **78** 085432
[55] Nilsson J, Castro Neto A H, Guinea F and Peres N M R 2006 *Phys. Rev. Lett.* **97** 266801
Nilsson J, Castro Neto A H, Guinea F and Peres N M R 2008 *Phys. Rev.* B **78** 045405
[56] Abergel D S L and Fal'ko V I 2007 *Phys. Rev.* B **75** 155430
[57] Nicol E J and Carbotte J P 2008 *Phys. Rev.* B **77** 155409
[58] Wang X, Zhi L and Müllen K 2008 *Nano Lett.* **8** 323
[59] Wu J, Becerril H A, Bao Z, Liu Z, Chen Y and Peumans P 2008 *Appl. Phys. Lett.* **92** 263302
[60] Blake P, Brimicombe P D, Nair R R, Booth T J, Jiang D, Schedin F, Ponomarenko L A, Morozov S V, Gleeson H F, Hill E W, Geim A K and Novoselov K S 2008 *Nano Lett.* **8** 1704
[61] Kuzmenko A B, van Heumen E, Carbone F and van der Marel D 2008 *Phys. Rev. Lett.* **100** 117401
[62] Schedin F, Geim A K, Morozov S V, Jiang D, Hill E H, Blake P and Novoselov K S 2007 *Nat. Mater.* **6** 652
[63] Meyer J C, Girit C O, Crommie M F and Zettl A 2008 *Nature* **454** 319
[64] Freitag M 2008 *Nat. Nanotechnol.* **3** 455
[65] Li X, Wang X, Zhang L, Lee S and Dai H 2008 *Science* **319** 1229
[66] Ponomarenko L A, Schedin F, Katsnelson M I, Yang R, Hill E W, Novoselov K S and Geim A K 2008 *Science* **320** 356
[67] Stampfer C, Güttinger J, Molitor F, Graf D, Ihn T and Ensslin K 2008 *Appl. Phys. Lett.* **92** 012102
[68] Stampfer C, Schurtenberger E, Molitor F, Güttinger J, Ihn T and Ensslin K 2008 *Nano Lett.* **8** 2378
[69] Silvestrov P G and Efetov K B 2007 *Phys. Rev. Lett.* **98** 016802
[70] Sols F, Guinea F and Castro Neto A H 2007 *Phys. Rev. Lett.* **99** 166803
[71] Wunsch B, Stauber T, Sols F and Guinea F 2008 *Phys. Rev. Lett.* **101** 036803
[72] Katsnelson M I and Guinea F 2008 *Phys. Rev.* B **78** 075417
[73] Recher P, Trauzettel B, Rycerz A, Blanter Ya M, Beenakker C W J and Morpurgo A F 2007 *Phys. Rev.* B **76** 235404
[74] Trauzettel B, Bulaev D V, Loss D and Burkard G 2007 *Nat. Phys.* **3** 192
[75] Recher P, Nilsson J, Burkard G and Trauzettel B 2008 arXiv:0810.0419
[76] Matulis A and Peeters F M 2008 *Phys. Rev.* B **77** 115423
[77] Zhang Z Z, Chang K and Peeters F M 2008 *Phys. Rev.* B **77** 235411
[78] Chen H-Y, Apalkov V and Chakraborty T 2007 *Phys. Rev. Lett.* **98** 186803
[79] Wang X, Ouyang Y, Li X, Wang H, Guo J and Dai H 2008 *Phys. Rev. Lett.* **100** 206803
[80] Brey L and Fertig H A 2006 *Phys. Rev.* B **73** 235411
[81] Son Y-W, Cohen M L and Louie S G 2006 *Phys. Rev. Lett.* **97** 216803
[82] Castro E V, Peres N M R and Lopes dos Santos J M B 2008 *J. Optoelectron. Adv. Mater.* **10** 1716
[83] DiVincenzo D P and Mele E J 1984 *Phys. Rev.* B **29** 1685
[84] Ribeiro R M, Peres N M R, Coutinho J and Briddon P R 2008 *Phys. Rev.* B **78** 075442
[85] Giovannetti G, Khomyakov P A, Brocks G, Kelly P J and van den Brink J 2007 *Phys. Rev.* B **76** 73103
[86] Lu Y H, He P M and Feng Y P 2007 arXiv:0712.4008
[87] Gomes J V and Peres N M R 2008 *J. Phys.: Condens. Matter* **20** 325221
[88] Cheianov V V and Fal'ko V I 2006 *Phys. Rev.* B **74** 041403
[89] Alberto P, Fiolhais C and Gil V M S 1996 *Eur. J. Phys.* **17** 19
[90] Fogler M M, Glazman L I, Novikov D S and Shklovskii B I 2008 *Phys. Rev.* B **77** 075420
[91] Berry M V and Mondragon R J 1987 *Proc. R. Soc. Lond.* A **412** 53
[92] Akhmerov A R and Beenakker C W J 2008 *Phys. Rev.* B **77** 085423
[93] Castro E V, Peres N M R, Lopes dos Santos J M B, Castro Neto A H and Guinea F 2008 *Phys. Rev. Lett.* **100** 026802
[94] Zhao L and Yelin S F 2008 arXiv:0804.2225v1 [cond-mat.other]
[95] Hentschel M and Guinea F 2007 *Phys. Rev.* B **76** 115407
[96] Wunsch B, Stauber T and Guinea F 2008 *Phys. Rev.* B **77** 035316
[97] Cserti J, Palyi A and Peterfalvi C 2007 *Phys. Rev. Lett.* **99** 246801
[98] Hewageegana P and Apalkov V 2008 *Phys. Rev.* B **77** 245426
[99] Rabi I I 1928 *Z. Phys.* **49** 507
[100] Stampfer C, Schnez S, Guettinger J, Hellmueller S, Molitor F, Shorubalko I, Ihn T and Ensslin K 2008 arXiv:0807.2710v1
[101] Schliemann J 2008 *New J. Phys.* **10** 043024
[102] Wakabayashi K, Fujita M, Ajiki H and Sigrist M 1999 *Phys. Rev.* B **59** 8271
[103] Dong S-H and Ma Z-Q 2003 *Phys. Lett.* A **312** 78
[104] Janssens K L, Partoens B and Peeters F M 2001 *Phys. Rev.* B **64** 155324
[105] Averin D V and Likharev K K 1991 *Mesoscopic Phenomena in Solids* ed B L Altshuler, P A Lee and R A Webb (Amsterdam: Elsevier)
[106] Grabert H and Devoret M H (ed) 1992 *Single Electron Tunneling* (New York: Plenum)
[107] Ferńandez-Rossier J, Palacios J J and Brey L 2007 *Phys. Rev.* B **75** 205441
Fernández-Rossier J and Palacios J J 2007 *Phys. Rev. Lett.* **99** 177204
[108] Abramowitz M and Stegun I A 1965 *Handbook of Mathematical Functions* (New York: Dover)
[109] Berggren K-F, Roos G and van Houten H 1988 *Phys. Rev.* B **37** 10118
[110] Peres N M R, Castro Neto A H and Guinea F 2006 *Phys. Rev.* B **73** 241403
[111] Bhowmick S and Shenoy V B 2008 *J. Chem. Phys.* **128** 244717
[112] Kühner T D and White S R 1999 *Phys. Rev.* B **60** 335
[113] Peres N M, Guinea F and Castro Neto A H 2005 *Phys. Rev.* B **72** 174406
[114] Nilsson J, Castro Neto A H, Peres N M and Guinea F 2006 *Phys. Rev.* B **73** 214418
[115] Dharma-wardana M W C 2007 *Phys. Rev.* B **75** 075427
[116] Peres N M R and Stauber T 2009 in preparation